Desert Dust Storms: Insurability and Financial Solutions*

September 2025

Andreas Milidonis
University of Cyprus,

Marina Solomou
University of Cyprus,

Panayiotis Kouis
University of Cyprus,

Petros Mouzourides
University of Cyprus,

Marina Neophytou
University of Cyprus

*We acknowledge financial support from the A.G. Leventis Foundation. We thank participants at the 2025 World Risk & Insurance Economics Congress, the QFRA symposium (2025) the 6^{th} European Actuarial Journal Conference (2024) and the 23^{rd} International Conference CREDIT (2024) for their valuable feedback. We also thank seminar participants at the Southern University of Science and Technology, Shaun Wang and Stavros Zenios for their constructive input. All remaining errors are our own. Milidonis (andreas.milidonis@ucy.ac.cy; contact author) and Solomou (solomou.marina@ucy.ac.cy) are from the Department of Accounting and Finance, of the University of Cyprus; Kouis (kouis.panayiotis@ucy.ac.cy) is from the Medical School of the University of Cyprus. Mouzourides (mouzourides.petros@ucy.ac.cy) and Neophytou (neophytou.marina@ucy.ac.cy) are from the Department of Civil and Environmental Engineering of the University of Cyprus.

Desert Dust Storms: Insurability and Financial Solutions

Abstract

How can societies financially mitigate the rising health risks of desert dust storms (DDS)? DDS are natural hazards that occur globally, with approximately half originating from the Sahara Desert. Using rural-background (RB) air-quality data from Southern Europe, located far away from anthropogenic influence, we identify *DDS days*, and document that daily deaths from respiratory and cardiovascular causes significantly increase in both Cyprus and Italy on days with PM_{10} concentration levels exceed location-specific thresholds. On extreme *DDS days*, the impact on mortality multiplies. DDS conditions and associated losses, meet key insurability criteria. We design a novel DDS catastrophe bond, and propose that it is offered through a coalition of countries exposed to DDS, enabling risk transfer to capital markets. We price the parametric CAT bond, using the occurrence of tail DDS events registered by RB stations. Our results challenge existing EU air quality standards, as we document substantial impact on public health at PM_{10} levels below the current EU low risk threshold of 50 μg/m^3, and inform public health and climate adaptation policy.

Keywords: Desert Dust Storms, Public Health, PM_{10}, Air Pollution, Insurance Innovation, Climate Finance.

JEL Classification: G22, G23, G38, I18, Q53, Q54.

1. Introduction

This latest Saharan dust episode is the third of its kind in the last two weeks and is related to the weather pattern that led to warmer weather across western Europe in recent days. The two previous episodes were mainly over the Mediterranean and southern Europe, although some effects such as deposition on people's cars occurred as far north as Scandinavia last weekend. Although it is not unusual for Saharan dust plumes to reach Europe, there has been an increase in the intensity and frequency of such episodes in recent years, which could potentially be attributed to changes in atmospheric circulation patterns.

Mark Parrington, CAMS Senior Scientist, April 2024

Poor ambient air quality due to elevated concentrations of particulate matter (PM) denotes a top-five health risk globally (Cohen et al., 2017). In 2020 alone, approximately 4.2 million deaths were attributed to PM exposure, while the associated economic cost was estimated at 2.7% of the gross world product (Romanello et al., 2021). The European Environmental Agency (EPA, 2022) identifies air pollution as Europe's most severe environmental health risk, correlated with amplified hospital admissions and excess premature deaths. Complementarily, the EPA report states that 96% of Europe's urban population is exposed to unhealthy levels of PM (Apte, Marshall, Cohen, & Brauer, 2015). While the global burden of disease related to Particulate Matter (PM) (Brauer et al., 2012; Organization, 2021) is well-documented in the medical and epidemiological literature (e.g.(Bell, Zanobetti, & Dominici, 2013; Shah & et al., 2015; Liu et al., 2019)), most studies center on long-term exposure of PM_{10} and $PM_{2.5}$ failing to differentiate between anthropogenic (e.g. industrial production) and natural PM emissions, (Mukherjee & Agrawal, 2017; Von Schneidemesser et al., 2015; Shao et al., 2011)), such as desert dust storms.

Desert Dust Storms (DDS) are natural hazards occurring worldwide , e.g. (Goudie, 2014; Mitsakou et al., 2008). They contribute to global dust emissions (United Nations ESCAP, 2018; Kok et al., 2021) and approximately half of them originate from the Sahara desert (Goudie & Middleton, 2006). Over 80% of the global dust load originates from deserts in North Africa and the Middle East (Lian et al., 2022), as Figure 1 suggests. Surprisingly, only 25% of the global dust emissions are attributable to anthropogenic activity (World

Health Organization, 2024), suggesting that approximately 75% of global dust emissions are driven by naturally-occurring reasons (Ginoux et al., 2012).

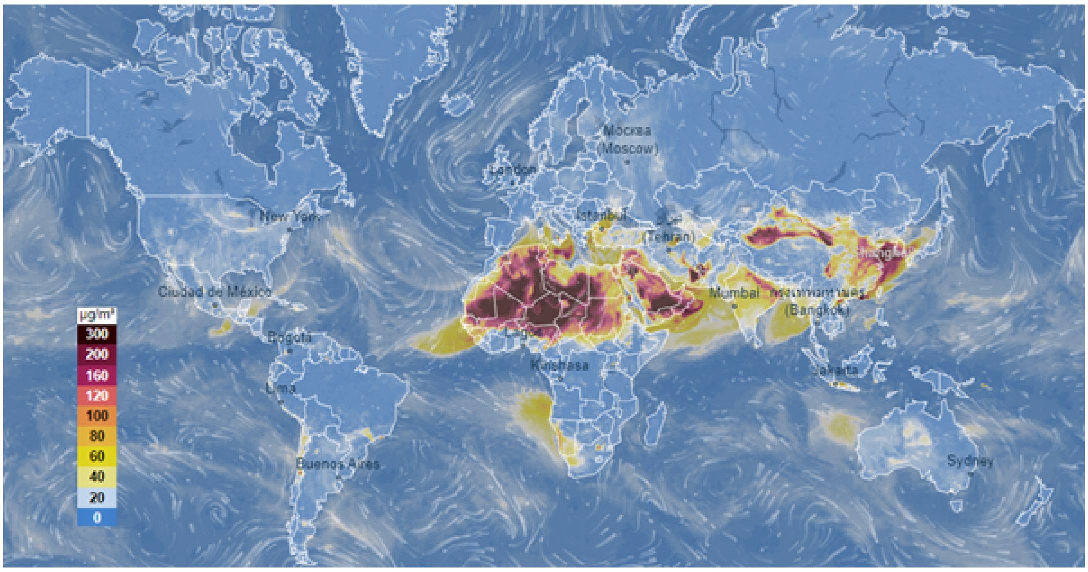

Figure 1: Daily PM_{10} measures for 29/3/2024 (Ventusky, 2024).

In this paper, we focus on the adverse effects of DDS on public health. Our novel approach allows to largely focus on natural (rather than anthropogenic) sources of dust emissions and their impact on the number of daily deaths. Similar to other natural hazards, our analysis shows that DDS satisfy risk insurability conditions (Kousky, 2019), such as randomness, determinability and measurability of DDS losses, limitation of moral hazard and adverse selection and pooling of losses. The insurability conditions allow us to propose and price a novel DDS Catastrophe bond, to mitigate the adverse effects of DDS on public health. Since public health in Southern Europe is primarily provided by the state, it is highly unlikely that individual insurance products will be developed to cover DDS. Hence, our proposal encourages regional collaboration across several countries to increase risk pooling and diversification, and consequently mitigate the adverse effects of DDS on public finances.[1] Transferring DDS vulnerability risk to capital markets enhances societal resilience and offers investors' diversification benefits.

We focus on Southern Europe, as it is directly impacted from dust originating from the Sahara desert and the Gulf region, providing at the same time granular data for the conduction of our analysis. To identify *DDS days* we employ the methodology of Achilleos et al. (2020) (see Appendix A), focusing on PM_{10} emissions from ground-level, rural-background

[1]Similar to the case of a developed private market, CAT bonds are expected to reduce tail risk associated with the natural hazard (Li & Su, 2024).

air-quality monitoring stations in conjunction with satellite measurements of air-quality components and supplementary meteorological readings such as wind direction, humidity and temperature. Rural stations are distinctly situated away from largely populated areas, minimizing exposure to anthropogenically induced PM_{10} emissions (Achilleos et al., 2014). Background stations measure the background levels of PM_{10} concentrations in the absence of anthropogenic activity and other events that might impact the recordings of PM_{10} (e.g. forest fires) (He, Schäfer, & Beck, 2022). Hence, rural-background (RB) stations serve as the state-of-the-art tool to measure PM_{10} emissions, largely from natural factors.

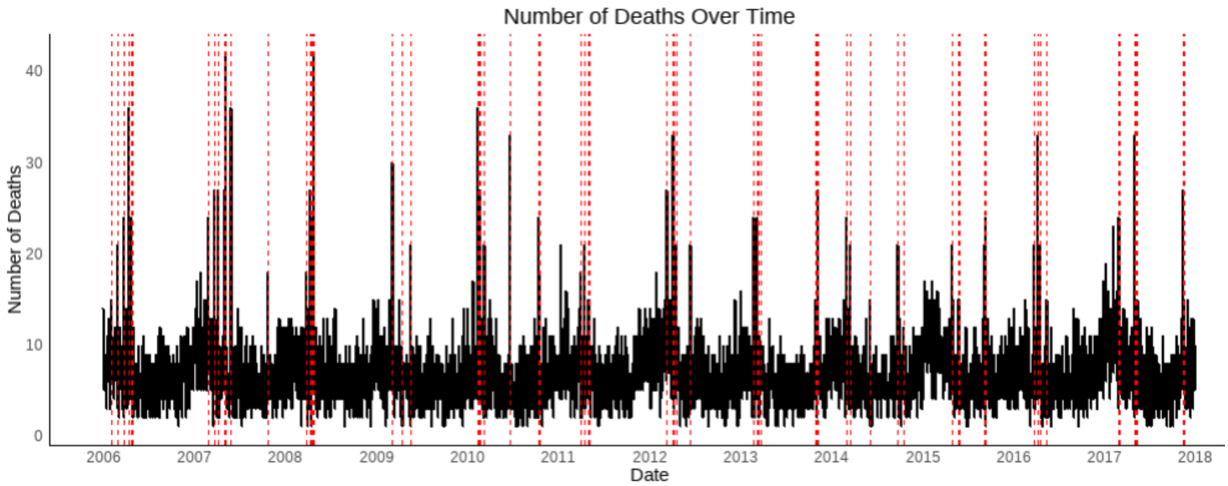

Figure 2: Daily number of deaths (all causes) in Cyprus (black line) vs. days impacted by DDS simultaneously (dotted red line) in three countries in Eastern Mediterranean (Greece, Cyprus and Israel), as identified by Achilleos et al. (2020)

We motivate our paper by focusing on the subset of *DDS days* (dotted red lines) that simultaneously impact the Eastern Mediterranean region; that is DDS events are recorded in Greece, Israel and Cyprus on the same day (Figure 2). We then plot the daily number of deaths (all causes; 2006-2017) in Cyprus. The graph suggests a correlation between major DDS and the number of daily deaths.

We build on this motivating evidence by conducting a systematic empirical analysis. We download daily, air-quality data from all RB stations in Southern Europe (S. K. Grange, 2021). We also request daily mortality data from respiratory and cardiovascular causes from all countries in Southern Europe (Cyprus and Italy have provided data). Our final sample represents about one-quarter of the population living in close proximity to RB stations in Southern Europe (about 17 out of 71 million people). In particular, our analysis starts from Cyprus (2007-2017), where in addition to daily death data, we also have data on daily hospitalizations from respiratory and cardiovascular causes. Following the epidemiological literature, we test whether daily death counts and hospital admissions are abnormally higher on *DDS days*. We find an increase in the number of daily deaths (hospital admissions) on *DDS days* by 3.8% (6.8%).

We then focus on days with extreme levels of PM_{10} levels to test if daily deaths and hospital admissions experience additional increases. We define "*Severe DDS days*" to be *DDS days* with PM_{10} level higher than the 99.5^{th} percentile of the PM_{10} distribution. We find that the impact of "*Severe DDS days*" is significantly larger than the respective impact of *DDS days* on the daily number of deaths, with their respective increases ranging from 3.8% to 17%. The effect on hospitalizations does not appear to differ.

We expand the analysis of *DDS days* on the daily number of deaths, by also using data from Italy. We propose and use an alternative, simpler definition for *DDS days*, specific to each RB station in Italy. Specifically, given that Achilleos et al. (2020) classify approximately 20% of the calendar days as DDS, and that PM_{10} levels constitute the most commonly used DDS proxy across earlier literature (Al-Hemoud et al., 2021; Y. Wang, Stein, Draxler, Jesús, & Zhang, 2011), we propose the following proxy: *DDS proxy days* are those days whose average daily PM_{10} level recorded, exceed the 80^{th} percentile of the corresponding historical distribution of daily PM_{10} levels at that RB station.[2]

The economic and statistical significance of the results in South-central Europe (Italy) are comparable to those of South-eastern Europe (Cyprus), suggesting generalizability of the results across Southern Europe. Additionally, in an extended sensitivity analysis, we discover that the daily number of deaths starts to increase at even lower PM_{10} levels than what our seemingly strict definition of *DDS proxy days* commands. Consequently, our results have public policy implications since daily deaths increase abnormally at levels of PM_{10} that the European Union considers to be the lowest risk category of air-quality.

To mitigate the expected financial cost associated primarily with the loss of lives from DDS, we propose and price a parametric, DDS catastrophe bond for a coalition of countries in Southern Europe. For simplicity, the DDS CAT bond will pay a fixed benefit (to the country in the coalition affected by a DDS event), proportional to the estimated parameter coefficient for each geographical region and the statistical value of life (Viscusi & Masterman, 2017). Such a benefit can finance, post-disaster, government assistance measures. The

[2]Results are robust to higher or lower thresholds.

trigger for each benefit payment is proposed to be a function of pre-determined PM_{10} levels, such as *DDS days* or on *Severe DDS days*. Such days are transparently identified through the recorded levels of PM_{10}, using RB air-quality stations.

Our proposal encourages regional collaboration across Southern European countries to enhance DDS risk pooling and diversification. A recent example of such a multi-country instrument was the earthquake CAT bond issued by the World Bank (Bank, 2023). Transferring DDS vulnerability risk to capital markets enhances societal resilience and offers investors diversification benefits.

In addition to mitigating DDS social vulnerability, the proposed DDS CAT bond will also be attractive to investors for the following reasons: (a) addition of a new natural hazard to capital markets, seemingly uncorrelated with CAT risks such as earthquake and hurricane risk; (b) additional geographical diversification, as the DDS exposure in Southern Europe will offer a new geographical addition to the global map of CAT risks; (c) given the randomness and rare nature of *Severe DDS days*, we expect a very low correlation of DDS CAT bonds and traditional investment opportunities like the S&P500 index.

Our results have public policy implications. The threshold of 50 $\mu g/m^3$ that the EU considers to be the lowest risk PM_{10} level for outdoor activity, does not adequately protect public health. Our results show abnormal increases in the daily number of deaths at levels significantly below 50 $\mu g/m^3$, which also vary by geographical region. While our paper focuses on Southern Europe, our approach can be applied in other DDS-prone regions around the world, such as Central and Eastern Asia, the Middle East, Sahara and parts of Australia (N. J. Middleton, 2017).

2. DDS Vulnerability, Insurability and Identification

2.1 DDS are natural hazards

There are two major types of PM pollution: anthropogenic and naturally-occurring. Anthropogenic emissions include, industrial activity, fuel consumption, local burning activities, local traffic activities and land use patterns. Naturally-occurring PM emissions are mainly due to DDS, but also due to forest fires and volcanic eruptions (Mukherjee & Agrawal, 2017; Von Schneidemesser et al., 2015; Maenhaut, Vermeylen, Claeys, Vercauteren, & Roekens, 2016). Southern European countries remain exposed to significant, naturally-occurring PM levels, due to their proximity to deserts in North Africa and the Arabian Peninsula (Shahsavani et al., 2012; Güllü, Ölmez, & Tuncel, 2000).

According to the World Meteorological Organization (WMO): [3] DDS are frequent meteorological hazards obtained in both semi-arid and arid regions. They are usually driven by either steep pressure gradients emerging in cyclones, or by turbulent winds. Such wind forces tend to raise large volumes of dust grains and sand particles from dry soils into the atmospheric body, transporting them for extended period of times and distance (hundreds of kilometers or more) away from their sources. The moving dust finally settles in random locations away from its source and it is recorded by ground level air-quality stations (measured at 1.8 meters above ground) (UNEP & WMO, 2016). During such events, recorded PM_{10} levels may significantly exceed the 2005 European Union (EU) daily threshold, value of $50\mu g/\ m^3$ (Koçak, Mihalopoulos, & Kubilay, 2007; Mitsakou et al., 2008) reaching levels close to $8000\mu g/\ m^3$ (Mamouri et al., 2016).

2.2 Insurability Conditions of Natural Hazards

Kousky (2019) outlines several conditions for insurability. The first condition necessitates

[3] See also the review article (J. X. Wang, 2015) and other methods to monitor DDS such as (O'Loingsigh et al., 2014)

that both the frequency and severity of DDS incurred losses should follow a random process. DDS are considered natural hazards that occur relatively frequently (about 20% chance per year) and have varying degrees of severity. Moreover, there is limited ex-ante predictability as to the precise geographic location of their initiation, their travel trajectory (in terms of longitude, latitude and altitude), their eventual point of landing and the actual cost on societies (through the generation of public health losses for the exposed populations).

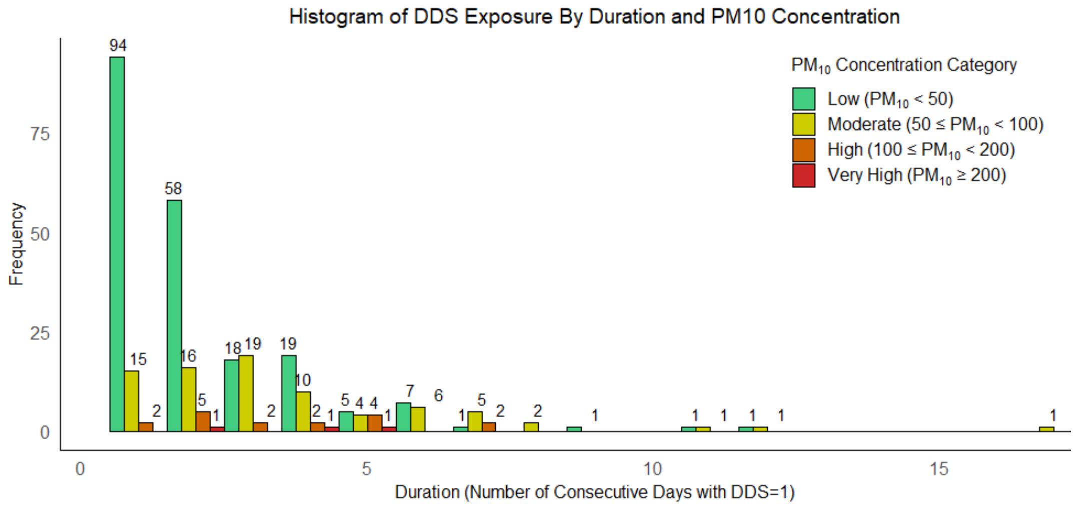

Figure 3: Histogram of DDS events (2006-2017) in Ayia Marina RB station classified by their duration and PM_{10} concentration category.

A second characteristic of insurability is that the risk should generate independent outcomes, and a thin-tailed probability distribution that can be quantified. Descriptive statistics of the daily frequency, severity and duration of DDS events point in that direction (see Figure 3: histogram of PM_{10} levels). While DDS events on average occur frequently, the presence of less frequent, more severe events generate a right tail on the PM_{10} distribution (He, Schäfer, & Beck, 2022). Given a DDS, there is still risk to be quantified with respect to the georgraphical area and population vulnerability to be affected from this DDS.

An insurable risk should also be associated with determinable losses. Since we focus on the impact of DDS on the daily number of deaths using parametric models from the epidemiological literature, that control for all factors potentially affecting death occurrences, then estimation of robust parameters allows to address this criterion.

Two additional conditions of insurable risk are the minimization of moral hazard and adverse selection. The random, independent nature of DDS events, ensures the mitigation of moral hazard concerns, as none of the two sides of the contract have incentives to shift risk to the other party of the contract. Moreover, none of them can affect the frequency or severity of a natural hazard like a DDS. Finally, it is highly unlikely for insured individuals to alter their behavioral patterns after entering the contract, as the largest part of the incurred loss due to DDS is a death benefit. [4] Adverse selection concerns are alleviated by the risk-pooling effect that applies when the entire population is covered, and the associated thin-tailed incurred loss distribution.

Finally, the issuance of a DDS related insurance contract necessitates sufficient demand and supply for insurance. On the demand side, our analysis documents a statistically and economically significant association between DDS and daily deaths in a representative part of Southern Europe. More importantly, we show that the impact on deaths starts at level of PM_{10} concentrations considered as low risk by the EU. These findings are likely to generate demand to mitigate DDS vulnerability for Southern European countries. On the supply side, a parametric CAT bond will offer additional diversification benefits to capital markets, across asset classes and geographical regions.

2.3 Economic Costs of DDS events

The literature lists several adverse effects on human health associated with PM_{10} exposure (Mukherjee & Agrawal, 2017; Organization, 2021). Examples include worsening ischemic heart disease (Zhang, Wang, & Wang, 2014), DNA degradation (Coronas et al., 2009) and increased preterm birth risk (Schifano et al., 2013). The literature has also widely documented the effect of PM pollution on both all-cause, cause-specific mortality and hospital admissions (Bell, Zanobetti, & Dominici, 2013; Atkinson & et al., 2014; R. W. Atkinson, Mills, Walton, & Anderson, 2015; Shah & et al., 2015; Liu et al., 2019).

Only a few studies have attempted to quantify economic costs associated with DDS (see Appendix B), such as (Ai & et al., 2008; Meibodi & et al., 2015; Miri & et al., 2009; Williams & Young, 1999; Jeong & et al., 2008; Pimentel & et al., 1995; Ekhtesasi & Sepehr, 2009). Such economic costs are associated with the adverse effects on human health, business activity, labor productivity, innovation, transportation, infrastructure and agriculture (including livestock health) (Ostro & et al., 2004; Cavalcanti, Mohaddes, Nian, & Yin, 2023; Tan & Yan, 2021; N. J. Middleton, 2017; Stefanski & Sivakumar, 2009; N. Middleton, 2024;

[4] Even in the case of hospital admissions (associated with much lower cost monetary cost than death) it is unlikely that claims will be manipulated, as claims will be paid at an aggregate level to the state (country) and not the individual.

Sivakumar, 2005; Schepanski, 2018).[5]

2.4 DDS identification: Rural, Background Stations

The exogenous nature of DDS allows to identify DDS by measuring increases of PM_{10} concentration, in environments with minimal potential contamination from other factors, such as anthropogenic PM_{10} emissions. The European Union (EU), implements a unified system to classify air monitoring stations, that accounts for the neighboring emmision sources of PM_{10} concentration (He, Schäfer, & Beck, 2022). The station classification codes include industrial, traffic, urban, sub-urban, background and rural.

By definition, rural stations are situated at a large distance from urban areas, to ensure that anthropogenically produced PM_{10} emissions have minimal impact on rural station measurements (Achilleos et al., 2014). As far as background stations are concerned, their primary objective is to measure the typical (background) levels of PM_{10} without being affected by anthropogenic activities and other events that might impact the recordings of PM_{10} (e.g. forest fires) (He, Schäfer, & Beck, 2022; Parliament & of the European Union, 2008). Consequently, we use measurements from ground-level, rural-background (RB) air-quality monitoring stations, to identify abnormal PM_{10} levels, driven primarily from naturally occurring sources.

2.4.1 Southeastern Europe

We start from the East side of Southern Europe, by using the RB station in Cyprus (Figure 4). Panel (A) in Figure 4 provides a visual representation with all 3-day backward trajectories of the recorded DDS, ending at the respective RB station on 29/11/2010. [6] As indicated by the trajectory paths, the source of the identified DDS event are the Sahara Desert and the Arabian Peninsula. Panel (b) further illustrates that dust trajectories that took place over the following 30 day window, covering a much broader region than Cyprus.

The RB station in Cyprus, is not only relevant for the geographic NUTS-2 (Nomen-

[5]Examples of severe DDS events are one in Phoenix (Arizona, USA) in 2011 (National Geographic, 2011), and another one in Cyprus (2015) (CNN, 2011; NASA Earth Observatory, 2015), that resulted in flight cancellations and disrupting business activity.

[6]The trajectories were estimated via the Real-time Environmental Applications and Display sYstem (READY) (National Oceanic and Atmospheric Administration (NOAA), 2024), a web-based system developed and openly provided by the National Oceanic and Atmospheric Administration's (NOAA) Air Resources Laboratory (ARL) (Rolph, Stein, & Stunder, 2017).

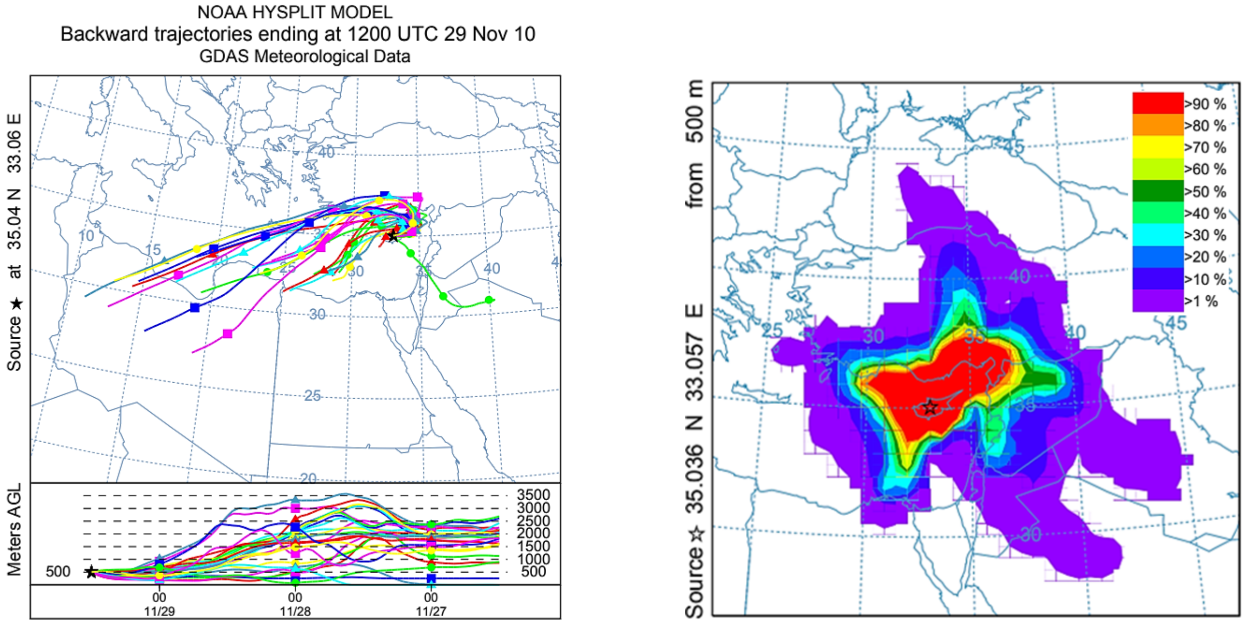

(a) **(b)**

Figure 4: Panel **(a)** illustrates the backward trajectory of the air mass at 12 UTC, at the site of Ayia Marina RB station (Cyprus). The box at the bottom of panel **a**, outlines different vertical air mass trajectories (in different colors) corresponding to estimated altitudes ranging from 500 m (AHL) to 3500 m (AGL). Panel **(b)** shows the trajectory frequencies over a 30-day time frame ranging from the 28/10/2010 - 19/11/2010 (Stein et al., 2015; Rolph, Stein, & Stunder, 2017).

clature of Territorial Units for Statistics) code in which it is located (i.e. the NUTS-2 code corresponds to the entire island-country of Cyprus), but also for the broader Eastern Mediterranean region (Baumbach & Pfeiffer, 2004; Kleanthous, Bari, Baumbach, & Sarachage-Ruiz, 2009). This is also evident from panel B of Figure 4, which shows that the depicted DDS event covers also the southern coast of Turkey, Northern Africa (i.e. Egypt) and other Middle Eastern countries such as Syria, Lebanon and Israel. [7] This station is part of the Co-operative Program for monitoring and Evaluation of the Long-range Transmission of Air Pollutants in Europe (EMEP) verifying the validity of the recorder measurements (Achilleos et al., 2014). The RB station in Cyprus is located in the Nicosia district with geographic coordinates $35^o02'08''N, 33^o03'26''E$. The Ayia Marina RB station is situated 40 km southwest of the capital of Cyprus, and it resides 450m above sea level.

[7] Based on our calculations, the total population in these areas ranges from 70-85 million people: about 25-30 million from Egypt; 25-30 million from Turkey; about 20-25 million from Israel, Lebanon, Syria and neighboring countries.

2.4.2 Southern Europe

We expand our coverage of PM_{10} concentration level data to other RB stations in Southern Europe, subject to data availability. We download all publicly accessible air-quality monitoring data from the air-quality e-reporting and European Commission's Airbase (AQER) depots.[8] We keep only the data from RB monitoring stations, which yields the stations illustrated in Figure 5. RB stations in Southern Europe are denoted in red dots while the rest of RB stations (from the rest of Europe are denoted in blue) Beck et al. (2025).

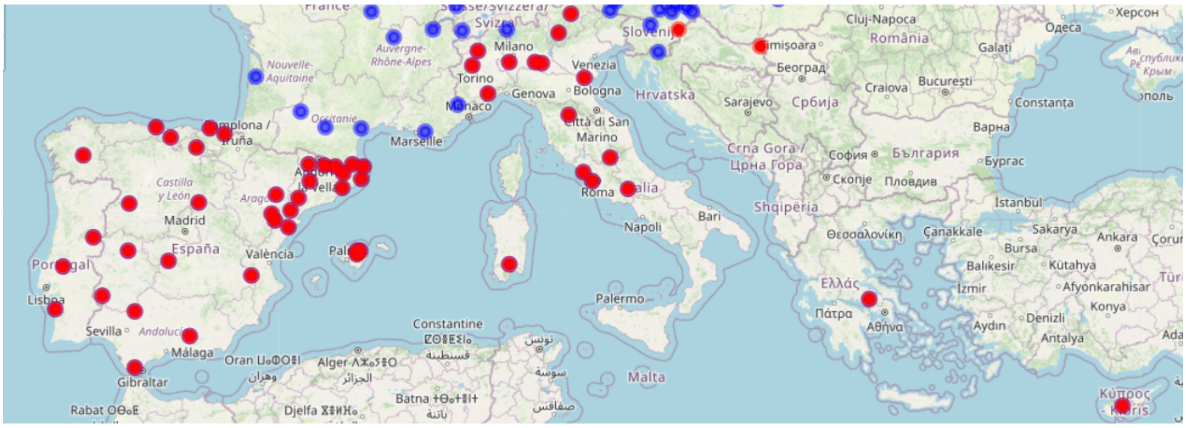

Figure 5: The rural-background (RB) stations (Parliament & of the European Union, 2008) in Southern Europe (red) and the remaining Europe (blue).

The majority of RB stations lies in Italy and Spain. The next step is to match PM_{10} data from RB stations in these two countries with the corresponding, regional meteorological data, such as daily averages of temperature, wind speed, wind direction and relative humidity, that the literature dictates (Elminir, 2005; Asimakopoulos, Flocas, Maggos, Vasilakos, & et al., 2012). Following this step, we then match with the key dependent variable, that is the daily number of deaths in each region (NUTS-2 code), and also daily hospital admissions where they exist, as described in the next section.

[8] We use the "`Saqgetr`" package, which interfaces with the Comprehensive R Archive Network (CRAN) to access all available datasets (S. Grange, 2019; Parliament & of the European Union, 2008)

3. Data and Descriptive Statistics

3.1 Daily Death and Hospital Admission Data

We requested mortality data from Cyprus, a representative sample of Southeastern Europe, along with Italy and Spain (by NUTS-2 code), denoting the two largest countries in Southern Europe with the largest number of RB stations. The acquired data include the daily number of deaths categorized due to cardiovascular (ICD10 codes I00 -I99) and respiratory (ICD10 codes J00 - J99) reasons (World Health Organization, 2019) codes, following the literature (Liu et al., 2019). We restrict our analysis to the period before 2019, to avoid contamination of the daily number of deaths from the COVID-19 outbreak, first recorded in Europe in early 2020 (Yuan et al., 2020).

We start our analysis from Cyprus for several reasons. First, we have a scientific definition of DDS days (Achilleos et al., 2020). Second, the RB station in Cyprus is the sole European RB station in the region covering the Eastern Mediterranean region. Third, the station is unlikely to be contaminated from neighboring countries, as they are quite far away from it (Turkey-110km; Syria-240km; Lebanon-250km; estimated using Google Earth). Fourth, Cyprus's data include both the daily number of deaths and hospital admissions (separately for respiratory and cardiovascular causes of disease; sources: Statistical Service of Cyprus and Ministry of Health, respectively).

We expand our analysis using the data from Italy to increase the generalizability of our results, via the incorporation of a larger population sample (we do not have data from Spain as of today). Mortality data for Italy was provided by the National Institute of Statistics of Italy (Istat) (Italian National Institute of Statistics (ISTAT), 2024) from January 2006 to December 2022. The total number of unique NUTS-2 codes in Italy, is 21 nonetheless but only 6 of them have at least one RB air-quality station. We further eliminate 2 of these NUTS-2 codes (ITC-2 (Valle d'Aosta) and ITH-2 (Provincia Autonoma di Trento)) as more than 50% of the PM_{10} observations are missing.

We propose a proxy for *DDS proxy days* in Italy, using the average daily PM_{10}

concentration; the most common factor of DDS definitions in the literature (e.g. Stafoggia et al. (2016); Al-Hemoud et al. (2021); Y. Wang, Stein, Draxler, Jesús, & Zhang (2011)). Moreover, according to Achilleos et al. (2020) we observe that about 20% of the days in their sample are classified as "DDS". Hence we define as *DDS proxy days* in RB stations in Italy, as those days with an average, daily, RB station specific PM_{10} level over the 80^{th} percentile of the corresponding RB station's distribution of daily PM_{10} levels.

NUTS-2 Code	Region Name	Population
CY00	Cyprus	875,899
ITC1	Piemonte	4,328,565
ITI4	Lazio	5,773,076
ITG2	Sardegna	1,622,257
ITH5	Emilia-Romagna	4,459,453
Total Sample Population		**17,059,250**

Table 1: The NUTS-2 codes included in our sample and the respective population level.

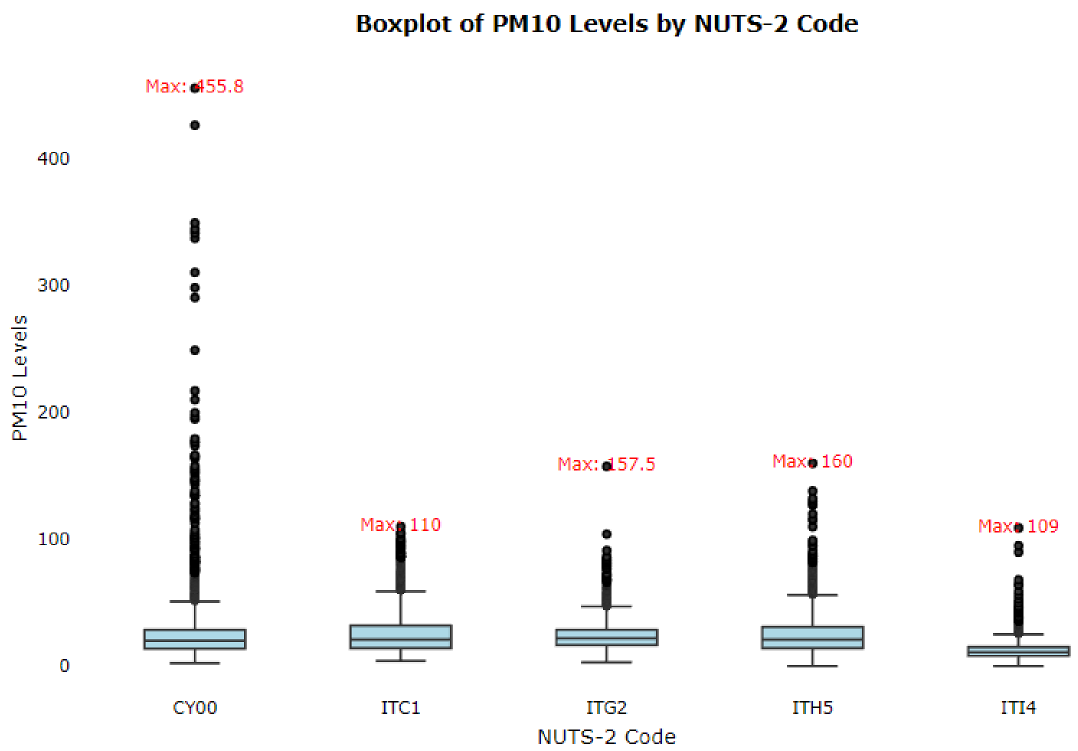

Figure 6: Box-plots of PM_{10} values for all sample NUTS-2 codes.

In total, our sample comprises five NUTS-2 codes outline in Table 1 along with their respective population (four from Italy and one from Cyprus), which represent approximately a quarter of the human population in all NUTS-2 codes with RB stations in Southern Europe (about 17 out of 71 million people). The PM_{10} distribution characteristics, namely minimum, maximum, median Q_2, first Q_1, and third Q_3, quartile values of each NUTS-2 region are shown in the box-plots illustrated in Figure 6. The interquartile range of CY00 distribution is relatively smaller compared to ITC1 and ITH5 codes indicating that the latter distribution experience greater variability within the middle 50% of the data, unlike ITI4 and ITG2 which show the opposite. On the other hand, Cyprus has more extreme values (echoing Mouzourides, Kumar, & Neophytou (2015)), with the maximum PM_{10} level registered at 455.8 $\mu g/m^3$, compared to the remaining NUTS-2 codes for Italy that record values of 110, 157.5, 160 and 109 $\mu g/m^3$ for each NUTS-2 code respectively.

3.2 Descriptive Statistics

Table 2, shows the descriptive statistics of the dependent and independent variables of our study. Dependent variables are the total daily deaths due to cardiovascular diseases *Deaths I*, total daily deaths due to respiratory causes of death *Deaths J*, and their sum *Total Deaths*.[9] The independent variables include PM_{10} levels, daily average relative humidity $Rel.Hum$, daily average temperature, $Temp$ and a binary DDS variable, that equals to one for days with DDS events and zero otherwise.

Table 2: Southeastern Europe: Descriptive statistics.

	N	*Min.*	*Max.*	*Mean*	*Median*	*Q1*	*Q3*	*Std. Dev*
Dependent								
Total Deaths	3960	0.00	23.00	6.64	6.00	5.00	8.00	2.90
Deaths. I	3960	0.00	18.00	5.44	5.00	4.00	7.00	2.53
Deaths. J	3960	0.00	12.00	1.20	1.00	0.00	2.00	1.18
Independent								
PM_{10}	3960	2.43	455.78	25.09	20.10	13.69	28.65	25.08
Rel.Hum	3960	14.08	91.56	53.45	55.25	42.83	64.59	14.47
Temp	3960	0.77	35.60	19.77	19.80	13.67	25.89	7.15
DDS	3960	0.00	1.00	0.18	0.00	0.00	0.00	0.38

Total Deaths ranges from $1-23$ deaths per day with mean and median values of 6.64 and 6 respectively. The interquantile range falls within $5-8$ deaths per day and the standard deviation is approximately 2.9 deaths per day. The independent variables reported include PM_{10} levels, Relative Humidity *Rel.Hum*, temperature *Temp* and a binary variable realising the value 1 for the days exhibiting a Desert Dust Storm and 0 otherwise. The

[9] We report descriptive statistics for hospitalizations in the appendix.

mean and median values of daily PM_{10} concentrations with units $\mu g/m^3$ are 25.09 and 20.10 respectively with the estimates ranging from 2.43 up to 455.78. The interquantile range spans from 13.69 up to 28.68 and the standard deviation is approximately 25.08. Additionally, the mean $Temp$ value is recorded to be $19.77°C$ over the examined period with minimum and maximum records of $0.77°C$ and $35.6°C$ and standard deviation of $7.15°C$. Finally, the binary DDS variable has a mean value of 0.18 suggesting that for approximately 18% of the total sample days are classified as *DDS days*.

Table 3: Southeastern Europe: Frequency of *DDS days* per year, and average PM_{10} level for days with DDS=1 and DDS=0.

Year	Total Days with DDS=1	Total Average PM_{10} con. (μg/m^3)	Average PM_{10} con. for DDS=1 (μg/m^3)	Average PM_{10} con. for DDS=0 (μg/m^3)	P-value
2007	94	28.082	51.606	19.764	<0.001
2008	134	35.426	60.296	21.061	<0.001
2009	62	27.051	63.218	19.576	<0.001
2010	118	33.486	59.972	20.684	<0.001
2011	38	21.469	49.055	18.204	<0.001
2012	31	19.543	48.551	16.810	<0.001
2013	53	24.776	66.410	17.704	<0.001
2014	49	22.750	53.833	17.884	<0.001
2015	48	22.984	60.665	17.186	<0.001
2016	35	20.140	47.168	17.238	<0.001
2017	48	21.892	56.868	16.405	<0.001

In Table 3 we report the daily average PM_{10} concentration level for all calendar days per year (2007-2017), and also for those days characterized as DDS (*DDS=1*), and the rest of the days (*DDS=0*).[10] We note a statistically significant difference in the average PM_{10} concentration between days with and without DDS. On average, days with DDS have a higher PM_{10} concentration ranging of about 47.17-66.4 μg/m^3 (p-value<0.001 for all years).

[10]The DDS events "DDS days" for CY00 have been derived by the study of Achilleos et al. (2020)

4. Methodology and Results

4.1 Methodology: Generalized Additive Models

We follow the methodology of (Liu et al., 2019) to test the association between DDS and daily number of deaths. Specifically, we implement Generalized Additive Models with a quasi-Poisson regression[11]:

$$ln(\mu_t) = ln[E(Y_t)] = \alpha_0 + \sum_{i=1}^{p} f_i(X_{t,i}) + \beta DDS_t + \sum_{d=1}^{6} Dow_d + \sum_{s=1}^{3} Season_s \tag{4.1}$$

where Y_t denotes the count of deaths, on day t. Coefficient β estimates the effect of DDS on Y_t. $X_{t,i}$ denotes control variable i on day t (such as temperature and relative humidity), f_i is the respective smoothed function. We also control for day and season fixed effects, using Dow_d and $Season_s$, (Touloumi et al., 2006) (see Appendix C), respectively.

Given that DDS might take place on consecutive days, or that the potential impact of DDS on public health might take a few days to appear, we also test for, and incorporate the optimal lag structure following Liu et al. (2019). We also incorporate a natural spline function for the lagged temperature and a natural spline function for the relative lagged humidity to control for any non-linear weather condition effects (Bell, Dominici, & Samet, 2005; Dominici et al., 2006; Chen et al., 2017). Hence we adjust model 4.1 to include a cross-basis function following (Gasparrini, 2014) to become[12]:

$$ln(\mu_t) = ln[E(Y_t)] = \alpha_0 + \sum_{i=1}^{p} f_i(X_{t,i}) + \beta DDS_t + \sum_{l=1}^{q} \gamma_l DDS_{t-l} + \sum_{d=1}^{6} Dow_d + \sum_{s=1}^{3} Season_s \tag{4.2}$$

where $\sum_{l=1}^{q} \gamma_l DDS_{t-l}$ denotes the cross-basis function capturing lagged effects of DDS over a time-span of q days.

[11] We use the R software "mgcv" package. We also implement the same methodology to conduct the analysis for hospital admissions, available in Appendix D.

[12] We use the R software "dlnm" package.

4.2 Results: DDS days on daily deaths - Southeastern Europe

We run each model by RB station, given that the DDS definition varies by broad geographical region. We start our analysis from the RB station in Cyprus, because Achilleos et al. (2020) provide a clear definition of *DDS days* for this station. We show the results for the impact of *DDS days* on daily number of deaths, in three separate columns in Table 4, from January 2007 until December 2017.

In the first column we show the impact of DDS on the sum of deaths from respiratory and cardiovascular diseases. In the second (third) column we isolate the impact on deaths from respiratory (cardiovascular) diseases. The estimated coefficients in Panel A show a positive, statistically significant (p-value < 0.05) impact of *DDS days* on the daily number of deaths arising from both respiratory and cardiovascular causes. The size of the coefficient is also economically significant as the logarithm of total daily number of deaths increases by 0.037 on *DDS days* which translates to an increase of 3.8% in total daily deaths ($exp(0.037) \approx 1.038$). This effect appears to be driven primarily from deaths attributed to respiratory related causes of death as the respective increase in daily respiratory deaths amounts to 0.105 (p-value < 0.01) on *DDS days*. This coefficient translates to a 11.07% increase in actual deaths from respiratory diseases ($exp(0.105) \approx 1.1107$). On the other hand the impact on deaths from cardiovascular diseases is not significant.

We next focus on the impact that tail events have on the daily number of deaths. We do this by separating the *DDS days* variable into two mutually exclusive, binary variables: DDS_{mild} and DDS_{severe}. We define DDS_{mild} as all the *DDS days* with PM_{10} concentrations less than 165 $\mu g/m^3$, and DDS_{severe} as the remaining *DDS days* with daily PM_{10} concentrations equal to or above 165 $\mu g/m^3$. The 165 $\mu g/m^3$ threshold represents the 99.5^{th}% percentile of the PM_{10} distribution of the RB station in Cyprus. Hence we test whether the impact of these tail events differs from events happening with lower PM_{10} concentrations.

Table 4: Impact of DDS on daily deaths - Southeastern Europe. This table uses a Generalized Additive Model (GAM) regression for the examination of the impact of DDS on the daily count of deaths. The dependent variables include (a) the logarithm of the aggregated total of daily deaths subject to respiratory and cardiovascular diseases *Total Daily Deaths*, (b) the logarithm of daily number of deaths subject to cardiovascular diseases only *Cardiovascular*, (c) the logarithm of daily number of deaths subject to respiratory diseases *Respiratory*. The dataset ranges from January 2007 up to December 2017. Panel A reports the results of the binary parametric coefficient DDS that equals one on *DDS days* and zero otherwise. Panel B reports the results of the binary parametric coefficients DDS_{mild} and DDS_{severe}. The former variable is defined as all the *DDS days* from the original dataset with PM_{10} concentrations less 165 $\mu g/m^3$, whilst the latter is defined as the remaining *DDS days* with daily PM_{10} concentrations above the specified threshold. The non-linear effects of the lagged relative humidity and lagged temperature on the dependent variable are captured through the spline functions $s(RelHum_{lag1})$ and $s(Temp_{lag1})$ respectively. The model accounts for fixed effects related to the day of the week, season and year. The model's goodness of fit is quantified by the Deviance Explained. The coefficient estimate of each explanatory variable is reported along with the associated $p-$value in both Panel A and Panel B. *, **, and *** signify the statistical significance at the 10%, 5% and 1% level respectively. The analysis has been carried out using different threshold specifications and the incurred findings remain qualitatively the same.

Panel A

	Total Daily Deaths		Respiratory		Cardiovascular	
	Estimate	p-value	Estimate	p-value	Estimate	p-value
Parametric Coefficients						
Intercept	-4.438	0.281	-93.513	< .01 ***	14.714	0.001 ***
DDS	0.037	0.036 **	0.105	0.010 **	0.020	0.297
Smooth Terms						
s(RelHum_lag1)	1.001	< .01 ***	1.001	0.251	1.001	< .01 ***
s(Temp_lag1)	5.656	< .01 ***	3.577	< .01 ***	6.427	< .01 ***
Model Fit Statistics						
Adjusted R^2	0.144		0.081		0.110	
Deviance Explained	14.2%		7.18%		10.7%	
n	3820		3820		3820	

Panel B

	Total Daily Deaths		Respiratory		Cardiovascular	
	Estimate	p-value	Estimate	p-value	Estimate	p-value
Parametric Coefficients						
Intercept	-4.400	0.285	-93.512	< .01 ***	14.782	0.001 ***
DDS_{mild}	0.032	0.073 *	0.105	0.011 **	0.014	0.472
DDS_{severe}	0.161	0.034 **	0.112	0.544	0.173	0.037 **
Smooth Terms						
s(RelHum_lag1)	1.001	< .01 ***	1.001	0.251	1.001	< .01 ***
s(Temp_lag1)	5.837	< .01 ***	3.577	< .01 ***	6.576	< .01 ***
Model Fit Statistics						
Adjusted R^2	0.145		0.081		0.110	
Deviance Explained	14.3%		7.18%		10.8%	
n	3820		3820		3820	

Table 5: Impact of DDS on daily deaths with lags - Southeastern Europe. This table uses a Generalized Additive Model (GAM) regression for the examination of the impact of DDS on the daily death outcomes. The dependent variables include (a) the logarithm of the aggregated total of daily deaths subject to respiratory and cardiovascular diseases *Total Daily Deaths*, (b) the logarithm of daily number of deaths subject to respiratory diseases *Respiratory*, (c) the logarithm of daily number of deaths subject to cardiovascular diseases *Cardiovascular*. The dataset ranges from January 2007 up to December 2017. Panel A reports the results of the binary parametric coefficient DDS that equals one on *DDS days* and zero otherwise, along with the results of the $DDS_{crossbasis}$ indicator that captures the 4-day lagged effects of DDS on the dependent variable. Panel B reports the results of the binary parametric coefficients DDS_{mild} and DDS_{severe}. The former variable is defined as all the *DDS days* from the original dataset with PM_{10} daily concentrations less than 165 $\mu g/m^3$, whilst the latter is defined as the remaining *DDS days* with daily PM_{10} concentrations above the specified threshold. The 4-day lagged effects subject to DDS are captured by the binary variables $DDS_{crossbasis\ mild}$ and $DDS_{crossbasis\ severe}$ respectively. The non-linear effects of the lagged relative humidity and lagged temperature on the dependent variable are captured through the spline functions $s(RelHum_{lag1})$ and $s(Temp_{lag1})$ respectively. The model accounts for fixed effects related to the - day of the week, season and year. The coefficient estimate of each explanatory variable is reported along with the associated $p-$value in both Panel A and Panel B. *, **, and *** signify the statistical significance at the 10%, 5% and 1% level respectively. The analysis has been carried out using different threshold specifications and the incurred findings remain qualitatively the same.

Panel A

	Total Daily Deaths		Respiratory		Cardiovascular	
	Estimate	p-value	Estimate	p-value	Estimate	p-value
Parametric Coefficients						
(Intercept)	-3.904	0.349	-93.332	< .01 ***	16.219	< .01 ***
DDS	0.058	0.006 **	0.127	0.011 **	0.035	0.140
$DDS_{crossbasis}$	-0.014	0.085 *	-0.012	0.511	-0.011	0.218
Smooth Terms						
s(RelHum_lag1)	1.000	< .01 ***	1.001	< .01 ***	1.001	< .01 ***
s(Temp_lag1)	5.914	< .01 ***	3.602	< .01 ***	6.520	< .01 ***
Model Fit Statistics						
Adjusted R^2	0.144		0.081		0.108	
Deviance Explained	14.2%		7.2%		11%	
n	3816		3859		3829	

Panel B

	Total Daily Deaths		Respiratory		Cardiovascular	
	Estimate	p-value	Estimate	p-value	Estimate	p-value
Parametric Coefficients						
Intercept	-3.789	0.363	-97.954	< .01 ***	16.515	< .01 ***
DDS_{mild}	0.054	0.011 **	0.107	0.025 **	0.025	0.265
DDS_{severe}	0.181	0.039 **	0.075	0.702	0.221	0.013 **
$DDS_{crossbasis\ mild}$	-0.015	0.072 *	0.002	0.853	-0.006	0.320
$DDS_{crossbasis\ severe}$	-0.004	0.933	0.040	0.606	-0.045	0.238
Smooth Terms						
s(RelHum_lag1)	1.001	< .01 ***	1.001	0.159	1.000	< .01 ***
s(Temp_lag1)	6.101	< .01 ***	3.348	< .01 ***	4.907	< .01 ***
Model Fit Statistics						
Adjusted R^2	0.144		0.083		0.104	
Deviance Explained	14.3%		7.5%		10.6%	
n	3816		3628		3599	

We show the results for DDS_{severe} and DDS_{mild} in Table 5 Panel B. The estimated coefficients of DDS_{mild} and DDS_{severe} show a positive and statistical significant impact on the daily number of total deaths with p-value < 0.1 and p-value < 0.05, respectively. The expected increase of daily deaths on *Mild DDS days* equals 3.2% ($exp(0.032) \approx 1.0325$) whilst the increase in total daily deaths on *Severe DDS days* equals 17.5% ($exp(0.161) \approx 1.175$). The effect of DDS_{mild} appears to be driven primarily by daily deaths associated with respiratory diseases as the coefficient of DDS_{mild} is not significantly different from zero for cardiovascular deaths (p-value > 0.1). Also, the impact of DDS_{severe} is driven primarily by cardiovascular causes of death,[13] with a DDS_{severe} coefficient of 0.173, implying an increase of 18.9% in deaths from cardiovascular causes.

Results suggest that respiratory related daily deaths are more sensitive to DDS days with lower exposure to PM_{10} concentrations which appear to trigger an excessive amount respiratory related deaths equal to 11% ($exp(0.105) \approx 1.111$) compared to *non-DDS days*. On the other hand, unlike respiratory daily deaths, cardiovascular related deaths appear to be less sensitive to days with lower PM_{10} concentrations and only be impacted by days with higher values of PM_{10}, as depicted by DDS_{severe}.

We next show the results of the impact of DDS on the daily number of deaths, taking into account the potential lagged effect of DDS on deaths. We do this in Table 5 (Panel A) by incorporating a cross-basis function $DDS_{cross-basis}$ as specified in Equation 4.2. Results are consistent with those in Table 5. We note that the DDS coefficients in the three columns (total, respiratory and cardiovascular) appear higher when $DDS_{cross-basis}$ variable is introduced, whilst the DDS coefficient for cardiovascular-related deaths remains insignificant, as before. Specifically, the impact of DDS on the daily count of deaths from both causes, is estimated at 0.058 (p-value < 0.01) (vs. 0.037 in Table 5), which translates to about a 6% increase in the deaths ($exp(0.058) \approx 1.0597$). Similarly the impact of DDS on daily respiratory counts of deaths is weakly statistically significant (p-value < 0.1) and estimated to be 0.127 or 13.5% ($exp(0.127) \approx 1.135$) in deaths due to respiratory diseases.

Results for DDS_{mild} and DDS_{severe}, with lagged effects (i.e. $DDS_{crossbasis-mild}$ and $DDS_{severe\ crossbasis}$) are reported in Table 5 Panel B and are similar to those in Table 5, albeit stronger. Given that the coefficients of $DDS_{cross-basis}$ are not significant we keep a conservative view on these results and refer the reader to the results in Table 5. Specifically,

[13] DDS_{severe} is not statistically different than zero for respiratory related daily deaths.

the coefficient of DDS_{mild} is statistically significant (p-value < 0.05) for the number of total deaths from both causes and appears larger than the respective coefficient in Table 5 (0.054 vs. 0.032). Similarly, the coefficient of DDS_{severe} is statistically significant (p-value < 0.05) and equals to 0.181 (vs. 0.161 in Table 5).

Focusing next on the impact on deaths from respiratory causes in column two, we report that the DDS_{mild} coefficient is statistically significant (p-value < 0.05) and is equal to 0.107 (vs. 0.105 in Table 5). Similar to table 5, the coefficient for DDS_{severe} remains statistically insignificant. Regarding the impact of DDS on cardiovascular specific deaths, similar to Table 5, we document that the impact is driven more from DDS_{severe} than DDS_{mild} (not statistically significant). We note that the size of DDS_{severe} coefficient is 0.221 (vs. 0.167 in Table 5), which amounts to an increase of 24.7% ($exp(0.221) \approx 1.247$) in deaths from cardiovascular diseases.

In supplemental analysis (see Appendix D) we use Equations 4.1 and 4.2, to test the impact on hospital admissions in Cyprus. We document an overall increase in hospital admissions ranging from 5.0% to 9.0% from both causes associated with *DDS days*, which remains similar when lags are included. Conducting the analysis by type of cause, we find that for respiratory reasons, the coefficient of DDS_{mild} ranges between 0.085 to 0.075, and for DDS_{severe} ranges from 0.155 to 0.148. Respectively, the hospitalizations for cardiovascular reasons are linked to a DDS_{mild} coefficient between 0.051 to 0.029, while for DDS_{severe} they are not different than zero.

In sum, the impact of DDS on public health can be summarized as follows. For hospitalizations, we find an increase across both respiratory and cardiovascular diseases. When focusing on tail events, we observe an additional increase for respiratory causes but not for cardiovascular. Turning to the analysis on daily number of deaths, we find that DDS are associated with an overall increase in deaths from respiratory diseases, which multiply when the PM_{10} concentration is far in the right tail of the distribution. For deaths due to cardiovascular reasons, we find that they only happen when DDS have very high PM_{10} concentrations (which may be a complementary effect to hospitalizations).

4.3 Results: ***DDS proxy days*** on daily deaths in Southern Europe

Our analysis for Italy focuses on the four NUTS-2 codes, whose RB stations have sufficient PM_{10} and matching meteorological data to use. The four regions and their respective populations (Eurostat, 2024) are shown in Figure 7. We use an approximation for DDS days, *DDS proxy*, which corresponds to days with an average daily PM_{10} concentration equal to or higher than the 80^{th} percentile of the PM_{10} distribution. We use this percentile following the respective percentile of the empirical distribution of Achilleos et al. (2020), whose DDS definition uses the 82^{nd} percentile of the respective PM_{10} distribution.

For brevity, we summarize the results of our analysis in Figure 8, for each NUTS-2. Our dependent variable is the sum of daily deaths from respiratory and cardiovascular diseases of each NUTS-2 code. On the x-axis we plot the average daily PM_{10} concentration. The *DDS proxy* for each NUTS-2 station is shown using the gray dotted lines crossing the x-axis of each panel in Figure 8. On the y-axis we plot the value of the *DDS proxy* coefficient obtained from running Equation 4.1. As robustness checks, we also run Equation 4.1 using several other PM_{10} thresholds as proxies for DDS. We note that statistically significant coefficients are denoted by red dots.

Results in Italy confirm the results in Cyprus: the *DDS proxy* coefficient has a positive association with daily number of deaths from respiratory and cardiovascular diseases. This association is robust at even much lower levels than the 80^{th} percentile of the PM_{10} distribution. Another consistent result across Italy and Cyprus is that the DDS coefficient increases as the PM_{10} concentration increase (up to 0.15). Finally, the association between PM_{10} and deaths from respiratory and cardiovascular diseases starts from as low as $10\mu g/m^3$. These results provide additional evidence that the European Union might want to revise its "low risk" air-quality standards downwards, or consider region-specific standards (the EU "low risk" threshold is currently at $50\mu g/m^3$).

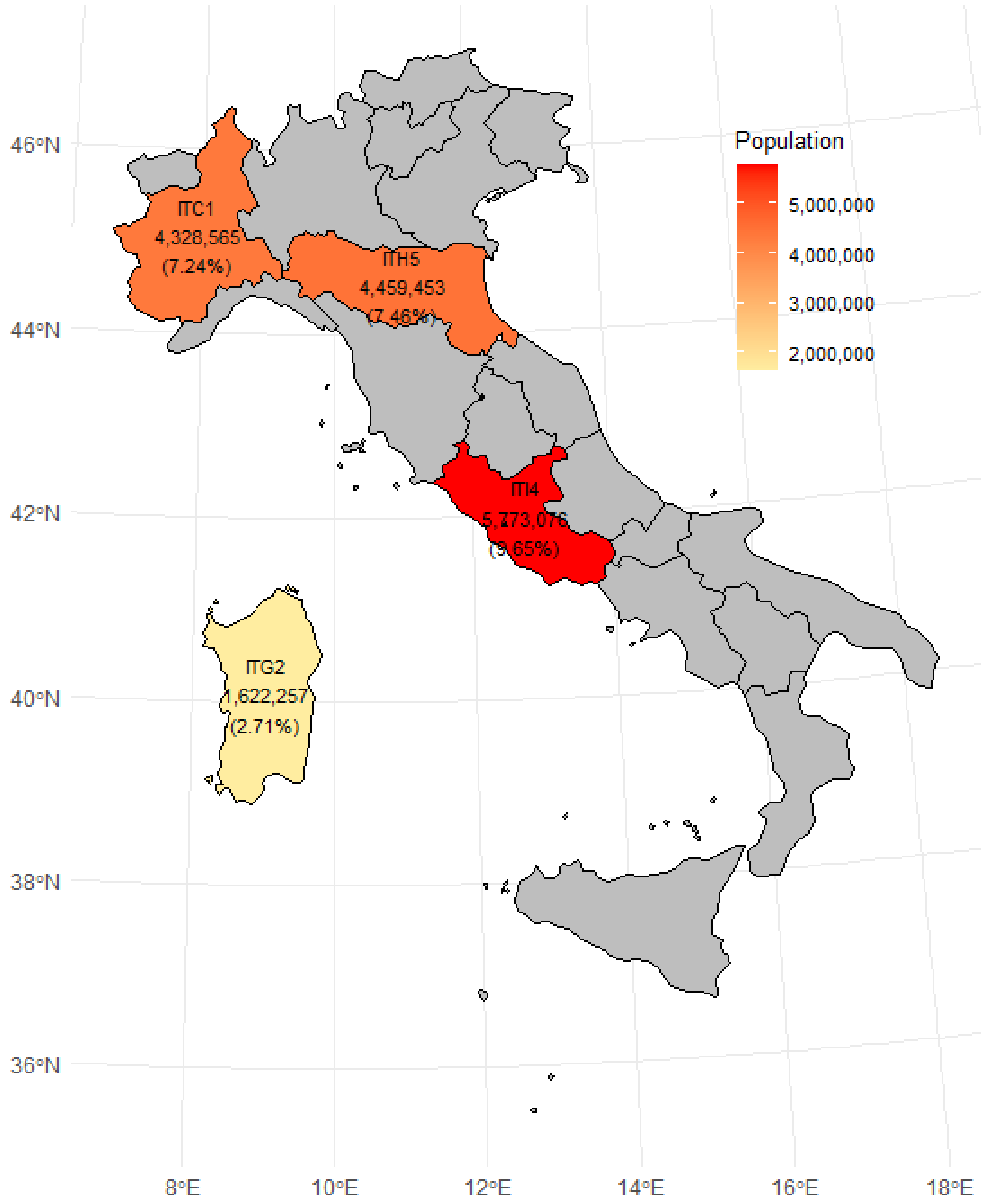

Figure 7: The NUTS-2 codes and respective geographic regions with rural-background stations (Parliament & of the European Union, 2008) and respective populations, in our sample.

Table 6: Impact of DDS on Daily Deaths by NUTS-2 Code - Southern Europe

The current table reports the Generalized Additive Model (GAM) regressions implemented for the examination of the impact of DDS on the total daily count of deaths. The dependent variables are the logarithm of the aggregated total of daily deaths subject to both respiratory and cardiovascular causes of death per NUTS-2 Code. The independent variables include the *DDS proxy* dummies equal to 1 for all sample days with daily average PM_{10} concentrations greater than the 80^{th} percentile, P_{80}, of each NUTS-2 specific PM_{10} distribution and zero otherwise. The non-linear effects of the lagged temperature and lagged relative humidity on daily deaths are approximated through the spline functions $s(\text{Temp}_{\text{lag1}})$ and $s(\text{RelHum}_{\text{lag1}})$ respectively. The dataset ranges from January 2006 up to December 2019. The model incorporates fixed effects related to the day of the week, season, and year. The estimated coefficients of each explanatory variable are reported along with the corresponding p-value. *, **, and *** signify statistical significance at the 10%, 5%, and 1% levels respectively. The underlined analysis has been conducted using various threshold specifications and the incurred findings remain qualitatively the same.

	ITG2		ITH5		ITI4		ITC1	
	Estimate	p-value	Estimate	p-value	Estimate	p-value	Estimate	p-value
Parametric Coefficients								
(Intercept)	-6.147	0.00550 **	2.595	0.0717 *	-17.84	< 0.001 ***	-5.468	< 0.001 ***
DDS proxy	0.021	0.0390 **	0.017	0.005 ***	0.031	< 0.001 ***	0.030	< 0.001 ***
Smooth Terms								
s(temp_lag1)	8.104	< 0.001 ***	6.548	< 0.001 ***	8.457	< 0.001 ***	7.632	< 0.001 ***
s(RH_lag1)	2.466	0.523	4.508	< 0.001 ***	5.738	0.00607 **	7.140	< 0.001 ***
Model Fit Statistics								
Adjusted R^2	0.262		0.386		0.460		0.408	
Deviance Explained	26.6%		39.4%		47.1%		41.9%	
n	3882		3818		3913		4215	

Table 7: Impact of DDS_{Mild} and DDS_{Severe} on daily Deaths by NUTS-2 Code - Southern Europe

The current table reports the Generalized Additive Model (GAM) regressions implemented for the examination of the impact of DDS_{Severe} and DDS_{Mild} on the total daily count of deaths. DDS_{Severe} is defined as all the sample days with average PM_{10} value > $P_{99.5}$ from which we subtract all days with average PM_{10} value > P_{80}, resulting into DDS_{Mild}. The dependent variables are the logarithm of the aggregated total of daily deaths subject to both respiratory and cardiovascular causes of death per NUTS-2 Code. The independent variables include the DDS dummies equal to 1 for all sample days with daily average PM_{10} concentrations greater than the 80^{th} percentile, P_{80}, of each NUTS-2 specific PM_{10} distribution and zero otherwise. The non-linear effects of the lagged temperature and lagged relative humidity on daily deaths are approximated through the spline functions $s(\text{Temp}_{\text{lag1}})$ and $s(\text{RelHum}_{\text{lag1}})$ respectively. The dataset ranges from January 2006 up to December 2019. The model incorporates fixed effects related to the day of the week, season, and year. The estimated coefficients of each explanatory variable are reported along with the corresponding p-value. *, **, and *** signify statistical significance at the 10%, 5%, and 1% levels respectively. The underlined analysis has been conducted using various threshold specifications and the incurred findings remain qualitatively the same.

	ITG2		ITH5		ITI4		ITC1	
	Estimate	p-value	Estimate	p-value	Estimate	p-value	Estimate	p-value
Parametric Coefficients								
(Intercept)	-5.957	0.007 ***	2.565	0.075 *	-17.83	< 0.001 ***	-5.510	< 0.001 ***
DDS_{Severe}	0.150	0.003 ***	0.139	< 0.001 ***	0.105	< 0.001 ***	0.031	0.265
DDS_{Mild}	0.017	0.098 *	0.014	0.022 **	0.028	< 0.001 ***	0.030	< 0.001 ***
Smooth Terms								
s(temp_lag1)	7.947	< 0.001 ***	6.497	< 0.001 ***	8.426	< 0.001 ***	7.612	< 0.001 ***
s(RH_lag1)	3.495	0.222	4.548	< 0.001 ***	5.497	0.0109 **	7.172	< 0.001 ***
Model Fit Statistics								
Adjusted R^2	0.266		0.390		0.460		0.407	
Deviance Explained	26.9%		39.7%		47.1%		41.8%	
n	3881		3817		3912		4215	

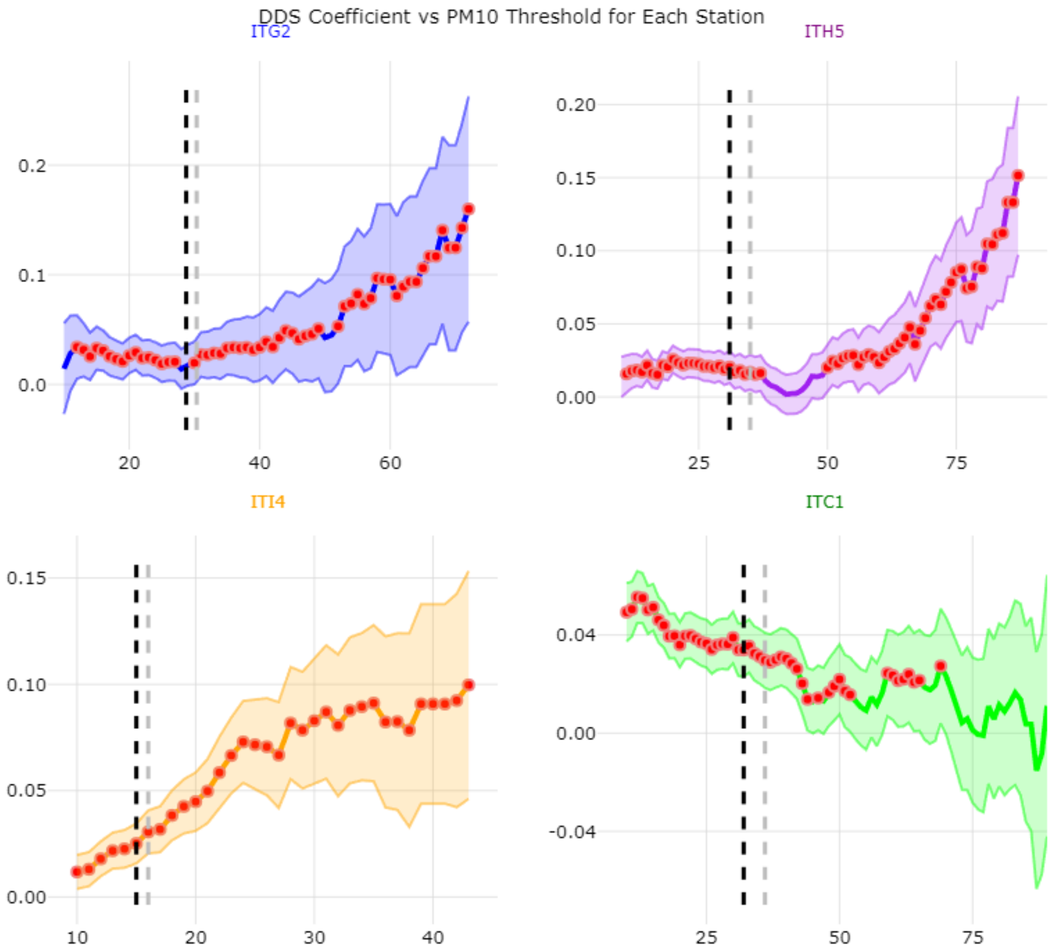

Figure 8: The impact of DDS on daily deaths from cardiovascular and respiratory deaths for Italy. The black and grey dotted vertical lines denote the 75^{th} and 80^{th} PM_{10} percentile, respectively. The PM_{10} threshold analysis starts from as low as $10\mu g/m^3$, for the identification of *DDS proxy days*. The corresponding DDS coefficients for each NUTS-2 code using Equation 4.1 are plotted on the vertical axis. Statistically significant coefficients are denoted by red dots.

For our DDS proxy coefficient, we report results comparable to Cyprus (Table 6). In particular, the estimated DDS coefficient for ITG2 is 0.021 (p-value = 0.039), for ITH5 0.017 (p-value = 0.005), for ITI4 0.031 (p-value <0.001) and for ITC1 0.030 (p-value <0.001).[14] We next conduct the analysis by focusing on tail events. $DDS_{Severe} = 1$ for all days with average daily $PM_{10} > P_{99,5}$ of each NUTS-2 specific PM_{10} distribution, and zero otherwise. Complementary, $DDS_{Mild} = 1$ for all days with average daily $PM_{10} > P_{80}$ excluding the DDS_{Severe} days, and zero otherwise. The incurred findings are reported in Table 7, and suggest that the DDS_{Severe} coefficients are positive and statistically significant (p-values <

[14]The same analysis is carried out using the GAM model specification outlined in Equation 4.2, incorporating the DDS lagged effects the results of which are robust and outlined in Appendix E.

0.010) remaining also qualitatively the same as the *DDS proxy* for all NUTS-2 codes except ITC1. We confirm that the DDS_{Severe} coefficient is significantly higher than the DDS_{Mild} coefficient, it extends up to 0.15 (p-values <0.001).

Results in Figure 8 confirm the increasing impact that higher levels of PM_{10} have on the daily number of deaths. We denote the 75^{th} and 80^{th} PM_{10} percentile, using the black and grey dotted vertical lines, respectively. We conduct the analysis at varying PM_{10} thresholds and denote with red dots any statistically significant coefficients obtained from Equation 4.1. We note that, while *DDS proxy* days are only set using the PM_{10} distribution of each RB station, statistically significant results start to appear at very low PM_{10} levels, such as $10\mu g/m^3$. More importantly, we document a positive relationship between PM_{10} levels and the impact on the daily number of deaths for three out of four NUTS-2 codes, which range up to about ten times the lowest recorded coefficient for the respective NUTS-2 code (e.g. ITI4).

5. Parametric DDS CAT Bond with a non-indemnity trigger

To mitigate the documented adverse effects of DDS events in Southern Europe, we propose the collaboration between a coalition of countries in Southern Europe (e.g. MED9) to offer a DDS, parametric Catastrophe (CAT) bond, that covers all NUTS-2 regions, with at least one RB station. Figure 9 illustrates the triggering mechanism of such a DDS CAT bond for the cases of Italy and Cyprus, where the DDS exposure of each NUTS-2 region denotes its corresponding contribution to the total DDS risk exposure. Thus, investors can contribute their capital into the Special Purpose Vehicle (SPV), and in the case where a DDS event occurs the analogous payment is triggered and covered by the privately raised capital, otherwise, the coalition of countries pay a return to investors through the SPV.

The proposed bond features a non-indemnity trigger (Cummins, 2008; Carpenter, 2006), that materializes in the case where, an RB station located in a specific NUTS-2 region of our sample, records a PM_{10} concentration level exceeding the 99.5^{th} percentile of the historical PM_{10} distribution of that RB-specific station. Once a bond payment is triggered, the payment amount is known with certainty in advance, and equals the expected economic cost incurred from the excess deaths subject to respiratory and cardiovascular causes in the respective NUTS-2 region, calculated using the parameters derived via Equation 4.2 at the 99.5^{th} percentile of the PM_{10} distribution. We structure the bond in such a way that multiple payment per NUTS-2 region are warranted within maturity, until full wipe-out occurs (see Section 5.2.1).

The Value Proposition related to the introduction of such a DDS CAT bond lies on the following reasons. First, countries in Southern Europe will attain access to risk mitigation funding from capital markets to address the adverse effect of *extreme* DDS on their populations and economies increasing economic resilience. Second, DDS denotes an additional diversifying peril for investors, not only across asset classes (i.e. compared to equities or fixed income) but also within natural hazard risks (as DDS losses are less likely to be correlated with losses from other catastrophes). Thus, the additional diversification benefit across catastrophe risks but also across geographic regions (i.e. Southern Europe), is likely to incentivize investors to accept a lower risk premium for the DDS CAT bond.

Our proposal regarding the development of a multi-country DDS CAT bond is inline with the 2018 Pacific Alliance Catastrophe Bond issued by the World Bank (World Bank Treasury, 2019), where different countries in Latin America (Chile, Colombia, Mexico and Peru) benefited from this CAT bond, through transferring part of their earthquake risk to capital markets (nominal value was US$1.36 billion) for a period of 2-3 years.

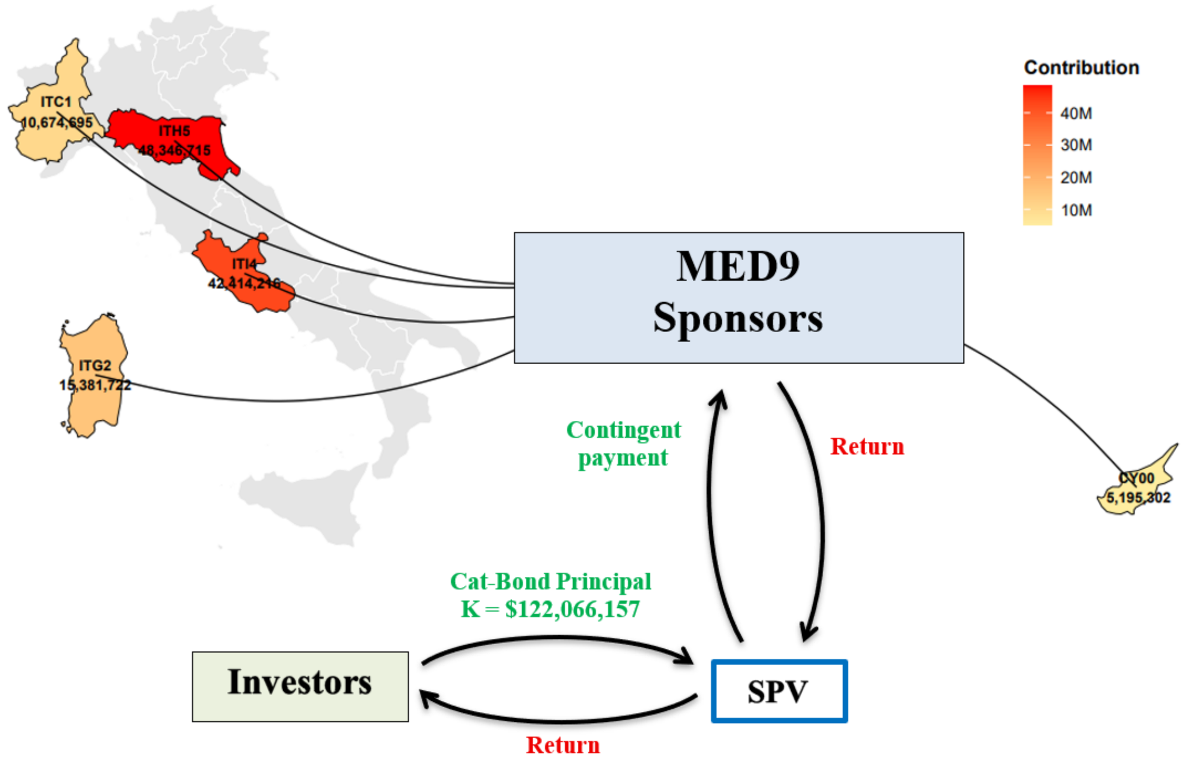

Figure 9: A graphical depiction of how DDS risk arising from each country (and specifically from each NUTS-2 region with an RB station) can be pooled together by a coalition of countries (e.g. Italy and Cyprus) to issue a parametric DDS CAT bond.

5.1 Parametric payment trigger

The payment trigger for the CAT Bond is parametric in nature and also tailored to each NUTS-2 region in our sample. It is activated when one or more RB stations, within an NUTS-2 regions, register a PM_{10} reading equal to or higher than the 99.5^{th} percentile of the PM_{10} distribution. We set the trigger to be NUTS-2 specific, as several confounding factors influence PM_{10} concentration levels such as, distance from the source (i.e. Deserts in North Africa or the Gulf region), altitude, temperature, humidity, etc. (Mouzourides, Kumar, & Neophytou, 2015).

According to Barrieu et al. (2024), parametric triggers facilitate high transparency and fast settlement. A potential drawback however includes the embedded high basis risk, that arises due to the relatively low correlation between payouts and insured losses. Nonetheless, in the proposed DDS Cat bond, the payment is set as a function of the estimated (historical) excess deaths from the extreme DDS, denotes a fixed measure and reduces basis risk (Teh & Woolnough, 2019).

5.2 Expected Payment amount

We focus initially on the NUTS-2 code of $CY00$ for the estimation of the expected payment amount attributable to the specific region. Given that DDS_{severe} is defined at the 99.5^{th} percentile of the PM_{10} distribution, we use the estimated DDS_{severe} coefficient for Cyprus obtained via Equation 4.1, denoted as $C_{DDS-severe_{CY00}}$. The incurred estimate implies a 17.5% ($exp(0.161) \approx 1.175$) increase in the number of daily deaths from respiratory and cardiovascular causes. Respectively, the average daily number of deaths related to the two causes of death for CY00 ($average\ death_{CY00}$) is 6.64, and the estimated Value of the Statistical Life (VSL_{CY00}) equals \$4,471,000. Hence, the estimated payment to be made to CY00 in the case where an extreme DDS event takes place is estimated to equal \$5,185,949 ($0.175 \times 6.64 \times 4,471,000$).

Analogously, Table D2 outlines all required inputs for the estimation of the contribution associated with each of the remaining NUTS-2 codes i, over the time period $[t, T]$. $V\bar{S}L_i(t, T)$ denotes the average expected Value of Statistical Life, and $C_{DDS-severe_i}$ denote the estimated coefficients derived from Equation 4.1. Finally, $\bar{d}_i(t, T)$ signify daily death values of each NUTS-2 code i over the CAT bond period $[t, T]$.

For simplicity, we assume that the proposed CAT bond provides coverage for up to one payment per NUTS-2 code over the maturity of the bond. Hence, under this assumption, each NUTS-2 code i, receives a payment of α times the estimated $Contribution_i$ in Table 8, where a denotes a multiplier of the maximum potential estimated loss.[15] Therefore, the maximum capital to be used (i.e. the principal value of the bond (K) which we set equal to the Price of the bond at issuance ($P_{t=0}$)) is obtained by the aggregated sum of all estimates in the $Contribution_i$ column of Table 11, which amounts to approximately \$122 million for

[15]For simplicity we proceed with the case of α=1, and later conduct a sensitivity analysis by relaxing this assumption.

a one-year contract.

Table 11: The contribution of each NUTS-2 region to the principal K of a DDS CAT bond (assuming $\alpha = 1$).

NUTS-2	$Population_i$	$V\bar{S}L_i$ (million \$)	$\boldsymbol{D\bar{D}S_{severe,i}}$	$\bar{d}_i$	$Contribution_i$ (\$)
CY00	875,899	4.471	0.161	6.64	5,185,949
ITG2	1,622,257	5.645	0.150	16.82	15,347,712
ITH5	4,459,453	5.645	0.139	57.48	48,386,982
ITI4	5,773,076	5.645	0.105	67.69	42,303,636
ITC1	4,328,565	5.645	0.031	61.00	10,841,875
$K = P_{t=0}$					**122,066,157**

5.2.1 Structure of DDS CAT Bond

The pricing framework employed follows closely the hybrid CAT bond structure developed by Tang & Yuan (2019). We assume independence between the financial market risk Q_1, and the catastrophe (DDS) risk Q_2. Thus, the total CAT bond risk Q is expressed as the convolution between two independent pricing measures. The former includes the risk neutral measure of the interest rate risk capturing the financial market performance of the bond Q_1, and the latter includes the DDS risk Q_2.[16]

The CAT bond price under the pricing measure Q, is the expectation of discounted future cash-flows, conditional on the evolution of the trigger process Y_t and the financial market performance over $[0, t]$. Hence, the CAT bond price, P_t, at time $t \epsilon [0, T]$ is:

$$\begin{aligned} P_t = K E_t^Q \Big[& \underbrace{\sum_{s=\lfloor t \rfloor + 1}^{\lfloor \tau \rfloor \wedge T} D(t,s)(R + i_s)\Pi(Y_{s-1})}_{\textit{Discounted sum of periodic coupon payments}} \\ & + \qquad \underbrace{D(t,\tau)\vartheta 1_{(\tau \leq T)}}_{\textit{Accrued coupon payment at wipe-out}} \\ & + \qquad \underbrace{D(t,T)\Pi(Y > T) 1_{(\tau > T)}}_{\textit{Remaining principal at maturity } T \textit{ if no wipe-out occurs}} \Big], \end{aligned} \tag{5.1}$$

where K and T denote the principal and maturity values of the CAT-bond respectively. R denotes the fixed annual coupon rate and i_t the floating coupon rate. $\Pi(Y) : [0, \infty) \rightarrow$

[16] Relaxing this assumption is beyond the scope of our paper but it can be developed in future research.

$[0,1]$ signifies a decreasing, right continued payoff function determined by the triggering process Y_t, such as $\Pi(0) = 1$. Similarly, τ indicates the time of a wipe-out such that $\tau = \inf\{t\epsilon\mathbb{R}_+ : \Pi(Y_t) = 0\}$. Assuming that the wipe-out takes place at time τ between two concurrent coupon payments, then an accrued coupon payment is being made to the investors, the value of which is determined by the period elapsed between the bond's issuance and τ, expressed by $\vartheta = (\tau - \lfloor\tau\rfloor)(R + i_t)\Pi(Y_{\lfloor\tau\rfloor})$. Similarly, in the case where no wipe-out occurs prior to T, investors receive the principal remaining on the maturity date T as a final redemption payment captured by $K(R + i_t)\Pi(Y)$. Finally, $D(t,s) = exp\left\{-\int_t^s r_u du\right\}$ is the discount factor corresponding to the time interval $[t,s]$. For simplicity, we assume no coupon payments for the DDS CAT-bond and instead, bond investors receive a fixed coupon rate R at maturity. Hence, the simplified equation for the DDS CAT bond price reduces to:

$$P_t = KE_t^Q\Big[D(t,\tau)\vartheta 1_{(\tau\leq T)} + D(t,T)\Pi(Y > T)1_{(\tau>T)}\Big]. \tag{5.2}$$

Under the assumption of independence between financial risk and DDS risk ($Q = Q_1 \times Q_2$), equation 5.2 becomes :

$$\begin{aligned} P_t =& KE_t^{Q_2}\Big[(\tau - \lfloor\tau\rfloor)\Pi(Y_{\lfloor\tau\rfloor})1_{(\tau\leq T)}E_t^{Q_1}\left[D(t,\tau)(R + i_t|\tau)\right]\Big] \\ &+ KE_t^{Q_2}\Big[\Pi(Y_T)E_t^{Q^1}\left[D(t,T)\right]\Big]. \end{aligned} \tag{5.3}$$

Following the general pricing framework above for a zero-coupon CAT bond, we proceed to incorporate the characteristics of the proposed DDS CAT bond. Specifically, we incorporate payment triggers and payment amounts for each NUTS-2 region. We price the bond assuming the face value of the bond at issuance equals the principal value of the bond. Given the unavailability of historical CAT bond pricing data, in order to infer the market price of risk κ, we provide an example of the bond using a range of κ values from the insurance pricing literature, from which we finally derive the corresponding bond returns (see Section 5.6).

The principal value of the bond with issuance date t and maturity date T, $K(t,T)$ is assumed to be a multiple of the maximum potential daily loss (α), capturing the case where all in-sample NUTS-2 codes simultaneously register a DDS_{severe} expressed as:

$$K(t,T) = a \sum_{i=1}^{\textit{all NUTS-2 codes}} C_{DDS_i\ severe} \times V\bar{S}L_i(t,T) \times \bar{d}_i(t,T)\ , \tag{5.4}$$

where $C_{DDS_i\ severe}$ denotes the $DDSsevere$ coefficient of each unique NUTS-2 region in sample i derived through Equation 4.1, $V\bar{S}L_i(t,T)$ denotes the average expected Value of Statistical Life of NUTS-2 code i over the time period $[t,T]$. Similarly, $\bar{d}_i(t,T)$ signify the daily death values of each NUTS-2 code i over the CAT bond period $[t,T]$.

In the current CAT-bond design we employ a non-indemnity parametric bond trigger that is activated with the occurrence of a DDS_{severe} event across any NUTS-2 code in the examined sample. Hence, the triggering process is assumed to follow a Markovian stochastic process expressed as follows:

$$\begin{aligned} Y(t,i) = a \sum_{i=1}^{\textit{all NUTS-2}} & \frac{C_{DDS_i\ severe} \times V\bar{S}L_i(t,T) \times \bar{d}_i(t,T)}{K} \\ & \times 1(PM_{10_{i,t}} \geqslant PM_{10_i^{99.5}}). \end{aligned} \tag{5.5}$$

Similarly, the pay-off function $\Pi(Y_{t,i})$, is approximated via:

$$\begin{aligned} \Pi(Y_{t,i}) &= \max\{a - Y_{t,i}, 0\} \\ &= \max\left\{ a - \frac{\sum_{i=1}^{\textit{all NUTS-2}} C_{DDS_i\ severe} \times V\bar{S}L_i(t,T) \times \bar{d}_i(t,T) \times 1\left(PM_{10_{i,t}} \geq PM_{10_i^{99.5}}\right)}{\sum_{i=1}^{\textit{all NUTS-2}} C_{DDS_i\ severe} \times V\bar{S}L_i(t,T) \times \bar{d}_i(t,T)}, 0 \right\}. \end{aligned} \tag{5.6}$$

5.2.2 Pricing Application

For simplification in the current pricing example, we employ the assumption that financial risk is time-invariant along with the values of all $NUTS-2$ specific parameters namely, $C_{DDS_i\ severe}$, $V\bar{S}L_i$, $\bar{P}_i$, and $\bar{d}_i$. For demonstration purposes, we initialize the principal value of the bond K, following equation 5.4, with $\alpha = 1$ such that $K = P_{(t=0)} \approx 115$ million euros indicating the face value of the bond $P_{t=0}$. Using historical DDS data, for each NUTS-2 code i in our sample, we estimate $\hat{\lambda}_i$ = *number of DDS events of sample period i /total days in sample period i*. This captures the DDS arrival intensity for each NUTS-2 code and analogously, the trigger probabilities p_i are estimated as $\hat{p}_i = \textit{number of } DDS_{severe,i}$ $/\textit{number of DDS of sample period } i$.

The trigger process of each NUTS-2 code $Y_{i,t}$, denotes a compound Poisson process with Bernoulli intensity and Poisson severity λ. Therefore, following the methodology of Tang & Yuan (2019), we implement the Wang transformation, factoring in different levels of catastrophe risk premium, κ, deriving an estimate of the corresponding trigger probability $\tilde{p}$ under the pricing measure Q_2, such that:

$$1 - \tilde{p} = \Phi(\Phi^{-1}(1 - p) - \kappa) \ . \tag{5.7}$$

To determine the annual bond rate R, the trigger development process of the CAT bond Y, is required to be determined as it establishes the principal allocation mechanism between the bond's sponsors and investors. In this example Y is specified as the superposition of all in sample NUTS-2 trigger processes Y_i as expressed by Equation 5.5.

For the determination of the optimal bond return R, we start by simulatng $10,000$ Poisson process paths with intensity $\hat{\lambda}\hat{p}$ for each NUTS-2 code i. Each process includes 365 time steps for equidistant values of $\kappa\epsilon[0, 0.8]$. For each simulation path $j\epsilon[1, 10,000]$ and time step $t\epsilon[0, 365]$, we cross-sectionally examine each $Y_i(j, t)$ and every time t there is a trigger event at any NUTS-2 code i in simulation number j, a corresponding economic loss of magnitude $C_{DDS_i\ severe} \times V\bar{S}L_i \times \bar{d}_i$ is subtracted from the principal amount. This process successfully captures the bond's payoff function as expressed by Equation 5.6, and derives the expected future value of the cat bond as the average across all $10,000$ simulations for every unique value of κ.

Finally, for the determination of the optimal annual bond return R, we employed the risk neutrality principle, that is, the discounted expected future value of the bond at maturity T, should equal to the principal K invested at a risk-free rate. Thus, assuming a constant risk free annual rate of 2%, we derive the optimal R for different values of $1 \leq \alpha \leq 3$ and κ as illustrated by Figure 10 (a). For the current example, where $\alpha = 1$, assuming that $\kappa = 0.8$, the corresponding optimal bond return date, is estimated to be $R \approx 17.5\%$ with a corresponding wipe out probability of $\approx 13,2\%$.

Table 9: Average annual number of DDS_{severe} across all 10,000 simulation paths of Wang-Adjusted trigger processes for different k values and NUTS-2 codes.

k	**CY00**	**ITC1**	**ITG2**	**ITH5**	**ITI4**
0.0	3.95	1.83	2.23	1.59	1.95
0.1	4.86	2.26	2.66	2.11	2.58
0.2	6.19	2.95	3.38	2.85	3.16
0.3	8.10	3.86	4.42	3.73	4.54
0.4	9.01	4.29	4.92	4.29	5.04
0.5	11.54	5.50	6.31	5.50	6.45
0.6	13.46	6.42	7.37	6.58	7.58
0.7	16.46	7.85	9.01	8.06	8.97
0.8	19.27	9.19	10.55	9.43	10.59
0.9	20.94	9.99	11.47	10.25	11.31
1.0	25.71	12.29	14.12	12.63	14.23

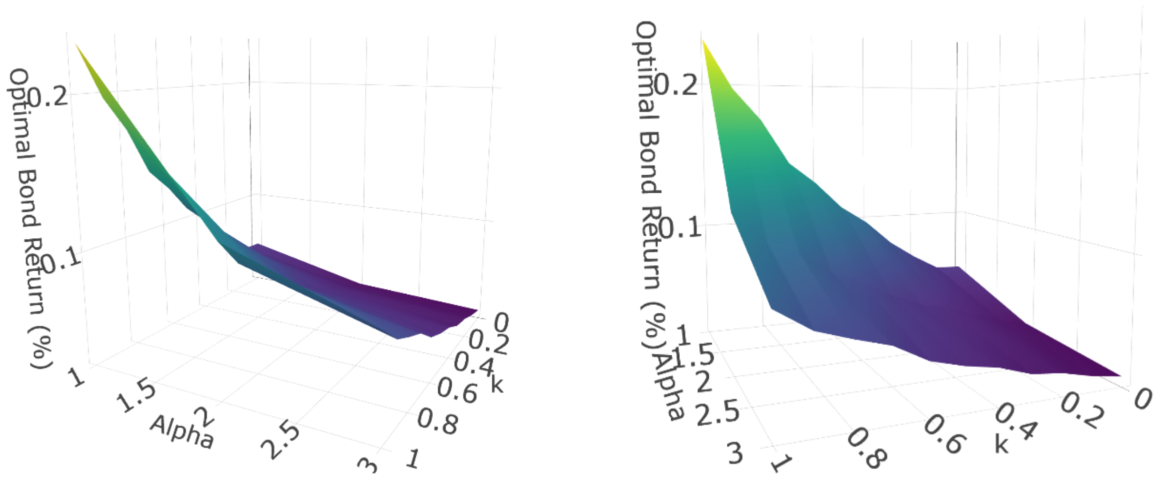

Figure 10 (a): Graphical illustration of the relation between Optimal Bond Return R with α and κ values.

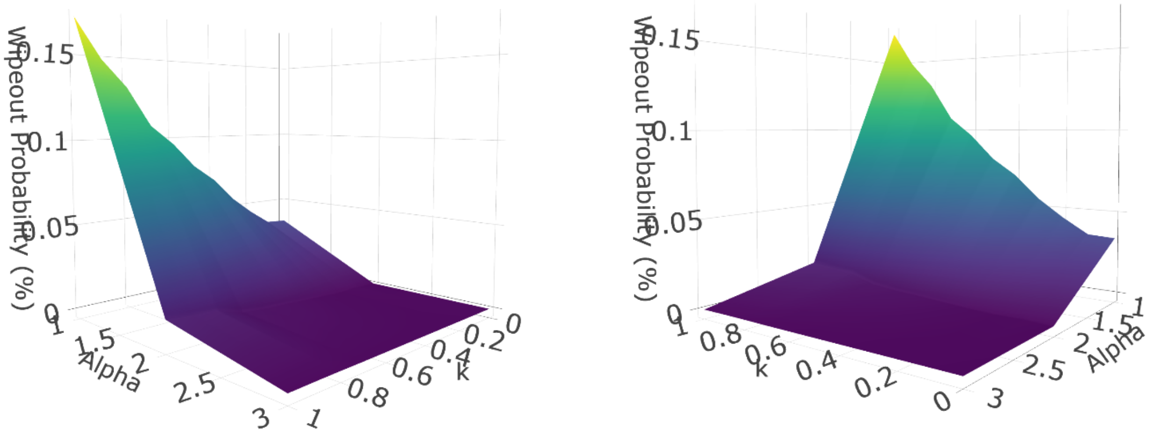

Figure 10 (b): Graphical illustration of the relation between Wipe-out Probability R with α and κ values.

6. Conclusion

Desert Dust Storms (DDS) are natural hazards impacting public health. We test the impact on DDS on public health using data from rural background, (RB) air-quality monitoring stations, which are far away from anthropogenic activity. PM_{10} concentration levels from natural sources, recorded by RB stations, are a key factor to identifying DDS. Given that half of DDS globally originate from the Sahara Desert, we focus on Southern Europe for our analysis. We start from a commonly accepted DDS definition in the environmental engineering literature, that corresponds to Southeastern Europe (Cyprus). Using this DDS definition, we document an economically significant increase in the daily number of deaths and hospital admissions on days identified as polluted by DDS. We then focus on severe DDS days (with a 0.5% probability of occurrence) for our analysis and find that the impact of the daily number of deaths quadruples.

We expand our analysis to other regions of Southern Europe to test for the generalizability of our results. Specifically, Italy and Spain, have the majority of RB stations in Southern Europe. Using matched data on the daily number of deaths from Italy, we expand our sample to represent about one quarter of the population in Southern Europe, that resides within broad geographical regions (i.e. NUTS-2 code) with RB monitoring stations. Because a DDS definition is derived subject to each specific monitoring station and given that there is no universal DDS definition in the literature for Italy, we use a proxy for DDS days (for each station) that corresponds to about the 80^{th} percentile of the distribution of historical PM_{10} concentration of that station. The results for Cyprus also generalize to Italy. We find that the daily number of deaths increases by a range of about 1.7% to 3.8% across all stations, and that the results for Italy are not sensitive to our definition for DDS for the Italian RB stations. More importantly, the impact that DDS have on the daily number of deaths in Italy, is documented to be a 5 to 10 times larger for rare DDS days (99.5% percentile of the distribution) than for more common ones (99.5% percentile) for three out of the four major geographical regions in Italy.

Following the documented results above, we argue that DDS events satisfy insurability conditions needed for considering underwriting insurance and financial products on

DDS risk. We propose and price a DDS CAT bond to cover Southern Europe. The introduction of DDS CAT bond improves diversification benefits for capital markets in two dimensions. First, DDS is a new, uncorrelated CAT risk relative to the existing pool of CAT risks covered by the CAT bond market. Second, DDS CAT bonds add to increase geographical diversification benefits to capital markets by including DDS risk in Southern Europe. Our proposed DDS CAT bond only focuses on a one-year period and only 25% of the NUTS-2 regions with RB stations. Hence the principal of the bond could well extend beyond 1 billion of the entire Southern Europe is covered over a period of about 3 years.

Our results also have implications for public policy. The most obvious implication is that the impact of DDS on the daily number of deaths starts at PM_{10} concentration levels that are below the European level of PM_{10} concentration that is considered safe. Moreover, the significantly higher impact on the daily number of deaths documented by more severe DDS, suggests that governments, at least in Southern Europe, should adopt a more systematic approach to warning local populations about forthcoming DDS episodes.

References

Achilleos, S., Evans, J. S., Yiallouros, P. K., Kleanthous, S., Schwartz, J., & Koutrakis, P. (2014). Pm10 concentration levels at an urban and background site in cyprus: the impact of urban sources and dust storms. *Journal of the Air & Waste Management Association*, *64*(12), 1352–1360.

Achilleos, S., Mouzourides, P., Kalivitis, N., Katra, I., Kloog, I., Kouis, P., ... et al. (2020). Spatio-temporal variability of desert dust storms in eastern mediterranean (crete, cyprus, israel) between 2006 and 2017 using a uniform methodology. *Science of the total environment*, *714*, 136693.

Ai, N., & et al. (2008). Socioeconomic impact analysis of yellow-dust storms: An approach and case study for beijing. *Economic Systems Research*, *20*(2), 187–203.

Al-Hemoud, A., Al-Khayat, A., Al-Dashti, H., Li, J., Alahmad, B., & Koutrakis, P. (2021). Pm2. 5 and pm10 during covid-19 lockdown in kuwait: Mixed effect of dust and meteorological covariates. *Environmental Challenges*, *5*, 100215.

Apte, J. S., Marshall, J. D., Cohen, A. J., & Brauer, M. (2015). Addressing global mortality from ambient pm2. 5. *Environmental science & technology*, *49*(13), 8057–8066.

Asimakopoulos, D., Flocas, H., Maggos, T., Vasilakos, C., & et al. (2012). The role of meteorology on different sized aerosol fractions (pm10, pm2. 5, pm2. 5–10). *Science of the total environment*, *419*, 124–135.

Atkinson, & et al. (2014). Epidemiological time series studies of pm2. 5 and daily mortality and hospital admissions: a systematic review and meta-analysis. *Thorax*, *69*(7), 660–665.

Atkinson, R. W., Mills, I. C., Walton, H. A., & Anderson, H. R. (2015). Fine particle components and health—a systematic review and meta-analysis of epidemiological time series studies of daily mortality and hospital admissions. *Journal of exposure science & environmental epidemiology*, *25*(2), 208–214.

Bank, W. (2023). *World bank executes its largest single-country catastrophe* *bond and swap transaction to provide chile $630 million in financial protection.* https://www.worldbank.org/en/news/press-release/2023/03/17/world-bank-executes-its-largest-single-country-catastrophe-bond-and-swap-transaction-to-provide-chile-630-million-in-fin. (Accessed: 2024-11-18)

Barrieu, P., Braun, A., & Makariou, D. (2024). Catastrophe bonds. In *Handbook of insurance: Volume i* (pp. 169–195). Springer.

Baumbach, G., & Pfeiffer, H. (2004). Preliminary assessment of ambient air quality in cyprus. *UNOPS project. Final report. Institute of Process Engineering and Power Plant Technology, Universitaet Stuttgart.*

Beck, C., Schäfer, B., & He, H. (2025). Spatial analysis of tails of air pollution pdfs in europe. *Environmental Data Science.*

Bell, M. L., Dominici, F., & Samet, J. M. (2005). A meta-analysis of time-series studies of ozone and mortality with comparison to the national morbidity, mortality, and air pollution study. *Epidemiology (Cambridge, Mass.)*, *16*(4), 436.

Bell, M. L., Zanobetti, A., & Dominici, F. (2013). Evidence on vulnerability and susceptibility to health risks associated with short-term exposure to particulate matter: A systematic review and meta-analysis. *American Journal of Epidemiology*, *178*(6), 865–876.

Brauer, M., Amann, M., Burnett, R. T., Cohen, A., Dentener, F., Ezzati, M., ... et al. (2012). Exposure assessment for estimation of the global burden of disease attributable to outdoor air pollution. *Environmental science & technology*, *46*(2), 652–660.

Carpenter, G. (2006). The catastrophe bond market at year-end 2005: ripple effects from record storms. *Guy Carpenter & Company, New York.*

Cavalcanti, T., Mohaddes, K., Nian, H., & Yin, H. (2023). *Air pollution and firm-level human capital, knowledge and innovation* (Working Paper No. 2304). Cambridge, UK: Faculty of Economics, University of Cambridge.

Chen, R., Yin, P., Meng, X., Liu, C., Wang, L., Xu, X., ... et al. (2017). Fine particulate air pollution and daily mortality. a nationwide analysis in 272 chinese cities. *American journal of respiratory and critical care medicine*, *196*(1), 73–81.

CNN. (2011). *Massive dust storm hits phoenix, arizona.* Retrieved from https://edition.cnn.com/2011/07/06/us/us-arizona-dust-storm/index.html (Accessed: 11-Feb-2025)

Cohen, A. J., Brauer, M., Burnett, R., Anderson, H. R., Frostad, J., Estep, K., ... et al. (2017). Estimates and 25-year trends of the global burden of disease attributable to ambient air pollution: an analysis of data from the global burden of diseases study 2015. *The lancet*, *389*(10082), 1907–1918.

Coronas, M. V., Pereira, T. S., Rocha, J. A., Lemos, A. T., Fachel, J. M., Salvadori, D. M., & Vargas, V. M. (2009). Genetic biomonitoring of an urban population exposed to mutagenic airborne pollutants. *Environment International*, *35*(7), 1023–1029.

Cummins, J. D. (2008). Cat bonds and other risk-linked securities: state of the market and recent developments. *Risk management and insurance review*, *11*(1), 23–47.

Dechezleprêtre, A., Rivers, N., & Stadler, B. (2019). *The economic cost of air pollution: Evidence from europe* (Tech. Rep. Nos. OECD Economics Department Working Papers, No. 1584). Paris: Organisation for Economic Co-operation and Development (OECD). doi: 10.1787/18151973

Dominici, F., Peng, R. D., Bell, M. L., Pham, L., McDermott, A., Zeger, S. L., & Samet, J. M. (2006). Fine particulate air pollution and hospital admission for cardiovascular and respiratory diseases. *Jama*, *295*(10), 1127–1134.

Draxler, R. R., Gillette, D. A., Kirkpatrick, J. S., & Heller, J. (2001). Estimating pm10 air concentrations from dust storms in iraq, kuwait and saudi arabia. *Atmospheric Environment*, *35*(25), 4315–4330.

Draxler, R. R., Ginoux, P., & Stein, A. F. (2010). An empirically derived emission algorithm for wind-blown dust. *Journal of Geophysical Research: Atmospheres*, *115*(D16).

Draxler, R. R., & Hess, G. (1998). An overview of the hysplit_4 modelling system for trajectories. *Australian meteorological magazine*, *47*(4), 295–308.

Ekhtesasi, M., & Sepehr, A. (2009). Investigation of wind erosion process for estimation, prevention, and control of dss in yazd–ardakan plain. *Environmental monitoring and assessment*, *159*, 267–280.

Elminir, H. K. (2005). Dependence of urban air pollutants on meteorology. *Science of the total environment*, *350*(1-3), 225–237.

EPA, U. S. E. P. A. (2022, august). *Health and environmental effects of particulate matter (pm).* https://www.epa.gov/pm-pollution/health-and-environmental-effects-particulate-matter-pm.

Escudero, M., Stein, A., Draxler, R., Querol, X., Alastuey, A., Castillo, S., & Avila, A. (2006). Determination of the contribution of northern africa dust source areas to pm10 concentrations over the central iberian peninsula using the hybrid single-particle lagrangian integrated trajectory model (hysplit) model. *Journal of Geophysical Research: Atmospheres*, *111*(D6).

Eurostat. (2024). *Population on 1 january by age and sex - nuts 3 regions.* https://ec.europa.eu/eurostat/databrowser/view/demo_r_d2jan/default/table. (Accessed: 2024-08-06)

Gasparrini, A. (2014). Modeling exposure–lag–response associations with distributed lag non-linear models. *Statistics in medicine*, *33*(5), 881–899.

Ginoux, P., Chin, M., Tegen, I., Prospero, J. M., Holben, B., Dubovik, O., & Lin, S.-J. (2001). Sources and distributions of dust aerosols simulated with the gocart model. *Journal of Geophysical Research: Atmospheres*, *106*(D17), 20255–20273.

Ginoux, P., Prospero, J. M., Gill, T. E., Hsu, N. C., & Zhao, M. (2012). Global-scale attribution of anthropogenic and natural dust sources and their emission rates based on modis deep blue aerosol products. *Reviews of Geophysics*, *50*(3).

Goudie, A. S. (2014). Desert dust and human health disorders. *Environment international*, *63*, 101–113.

Goudie, A. S., & Middleton, N. J. (2006). *Desert dust in the global system.* Springer Science & Business Media.

Grange, S. (2019). *saqgetr: Import air quality monitoring data in a fast and easy way.*

Grange, S. K. (2021). *saqgetr: Import air quality monitoring data in a fast and easy way.* Retrieved from https://github.com/skgrange/saqgetr (R package version

0.2.21)

Güllü, G. H., Ölmez, İ., & Tuncel, G. (2000). Temporal variability of atmospheric trace element concentrations over the eastern mediterranean sea. *Spectrochimica Acta Part B: Atomic Spectroscopy*, *55*(7), 1135–1150.

He, H., Schäfer, B., & Beck, C. (2022). Spatial heterogeneity of air pollution statistics in europe. *Scientific Reports*, *12*(1), 12215.

Hu, X., Lu, N., Niu, T., & Zhang, P. (2008). Operational retrieval of asian sand and dust storm from fy-2c geostationary meteorological satellite and its application to real time forecast in asia. *Atmospheric Chemistry and Physics*, *8*(6), 1649–1659.

Inness, A., Ades, M., Agustí-Panareda, A., Barré, J., Benedictow, A., Blechschmidt, A.-M., ... et al. (2019). The cams reanalysis of atmospheric composition. *Atmospheric Chemistry and Physics*, *19*(6), 3515–3556.

Italian National Institute of Statistics (ISTAT). (2024). *Istat - italian national institute of statistics.* Retrieved from https://www.istat.it/en/ (Accessed: 2024-08-06)

Jeong, D.-Y., & et al. (2008). Socio-economic costs from yellow dust damages in south korea. *Korean Soc. Sci. J*, *35*, 1–29.

Kleanthous, S., Bari, M. A., Baumbach, G., & Sarachage-Ruiz, L. (2009). Influence of particulate matter on the air quality situation in a mediterranean island. *Atmospheric Environment*, *43*(31), 4745–4753.

Koçak, M., Mihalopoulos, N., & Kubilay, N. (2007). Contributions of natural sources to high pm10 and pm2. 5 events in the eastern mediterranean. *Atmospheric Environment*, *41*(18), 3806–3818.

Kok, J. F., Adebiyi, A. A., Albani, S., Balkanski, Y., Checa-Garcia, R., Chin, M., ... et al. (2021). Contribution of the world's main dust source regions to the global cycle of desert dust. *Atmospheric Chemistry and Physics*, *21*(10), 8169–8193.

Kousky, C. (2019). The role of natural disaster insurance in recovery and risk reduction. *Annual Review of Resource Economics*, *11*, 399–418.

Li, H., & Su, J. (2024). Mitigating wildfire losses via insurance-linked securities: Modeling and risk management perspectives. *Journal of Risk and Insurance*, *91*(2), 383–414.

Lian, S., Zhou, L., Murphy, D. M., Froyd, K. D., Toon, O. B., & Yu, P. (2022). Global distribution of asian, middle eastern, and north african dust simulated by cesm1/carma. *Atmospheric Chemistry and Physics*, *22*(20), 13659–13676.

Liu, C., Chen, R., Sera, F., Vicedo-Cabrera, A. M., Guo, Y., Tong, S., ... et al. (2019). Ambient particulate air pollution and daily mortality in 652 cities. *New England Journal of Medicine*, *381*(8), 705–715.

Maenhaut, W., Vermeylen, R., Claeys, M., Vercauteren, J., & Roekens, E. (2016). Sources of the pm10 aerosol in flanders, belgium, and re-assessment of the contribution from wood burning. *Science of the Total Environment*, *562*, 550–560.

Mamouri, R.-E., Ansmann, A., Nisantzi, A., Solomos, S., Kallos, G., & Hadjimitsis, D. G. (2016). Extreme dust storm over the eastern mediterranean in september 2015: satellite, lidar, and surface observations in the cyprus region. *Atmospheric Chemistry and Physics*, *16*(21), 13711–13724.

Meibodi, A. E., & et al. (2015). Economic modeling of the regional polices to combat dust phenomenon by using game theory. *Procedia Economics and Finance*, *24*, 409–418.

Middleton, N. (2024). Impacts of dust storms on agriculture: A synthesis. In *E3s web of conferences* (Vol. 575, p. 05001).

Middleton, N. J. (2017). Desert dust hazards: A global review. *Aeolian research*, *24*, 53–63.

Middleton, N. J., Goudie, A. S., & Wells, G. L. (2020). The frequency and source areas of dust storms. In *Aeolian geomorphology* (pp. 237–259). Routledge.

Miri, A., & et al. (2009). Environmental and socio-economic impacts of dust storms in sistan region, iran. *International journal of environmental studies*, *66*(3), 343–355.

Mitsakou, C., Kallos, G., Papantoniou, N., Spyrou, C., Solomos, S., Astitha, M., & Housiadas, C. (2008). Saharan dust levels in greece and received inhalation doses. *Atmospheric Chemistry and Physics*, *8*(23), 7181–7192.

Mouzourides, P., Kumar, P., & Neophytou, M. K.-A. (2015). Assessment of long-term measurements of particulate matter and gaseous pollutants in south-east mediterranean. *Atmospheric Environment*, *107*, 148–165.

Mukherjee, A., & Agrawal, M. (2017). World air particulate matter: sources, distribution and health effects. *Environmental chemistry letters*, *15*, 283–309.

NASA Earth Observatory. (2015). *Dust storm sweeps across middle east.* Retrieved from https://earthobservatory.nasa.gov/images/86571/dust-storm-sweeps-across-middle-east (Accessed: 11-Feb-2025)

National Geographic. (2011). *Massive dust storm rolls into phoenix.* (Retrieved from https://www.nationalgeographic.com/science/article/110706-phoenix-dust-storm-haboob-arizona-picture-video)

National Oceanic and Atmospheric Administration (NOAA). (2024). *NOAA's HYSPLIT Atmospheric Dispersion Model.* Retrieved from http://www.ready.noaa.gov (Accessed: 2024-08-13)

Natsagdorj, L., Jugder, D., & Chung, Y. (2003). Analysis of dust storms observed in mongolia during 1937–1999. *Atmospheric Environment*, *37*(9-10), 1401–1411.

O'Loingsigh, T., McTainsh, G., Tews, E., Strong, C., Leys, J., Shinkfield, P., & Tapper, N. (2014). The dust storm index (dsi): a method for monitoring broadscale wind erosion using meteorological records. *Aeolian Research*, *12*, 29–40.

Organization, W. H. (2021). *Who global air quality guidelines: particulate matter (pm2. 5 and pm10), ozone, nitrogen dioxide, sulfur dioxide and carbon monoxide.* Author.

Ostro, W., & et al. (2004). *Outdoor air pollution: assessing the environmental burden of disease at national and local levels.* World Health Organization.

Parliament, E., & of the European Union, C. (2008). Directive 2008/50/ec of the european parliament and of the council of 21 may 2008 on ambient air quality and cleaner air for europe. *Official Journal of the European Union*, *152*, 1–44.

Pérez, C., Nickovic, S., Baldasano, J., Sicard, M., Rocadenbosch, F., & Cachorro, V. (2006). A long saharan dust event over the western mediterranean: Lidar, sun photometer observations, and regional dust modeling. *Journal of Geophysical Research: Atmospheres*, *111*(D15).

Pimentel, D., & et al. (1995). Environmental and economic costs of soil erosion and conservation benefits. *Science*, *267*(5201), 1117–1123.

Prospero, J. M., Ginoux, P., Torres, O., Nicholson, S. E., & Gill, T. E. (2002). Environmental characterization of global sources of atmospheric soil dust identified with the nimbus 7 total ozone mapping spectrometer (toms) absorbing aerosol product. *Reviews of geophysics*, *40*(1), 2–1.

Rolph, G., Stein, A., & Stunder, B. (2017). Real-time environmental applications and display system: Ready. *Environmental Modelling & Software*, *95*, 210–228.

Romanello, M., McGushin, A., Di Napoli, C., Drummond, P., Hughes, N., Jamart, L., ... Arnell, N. e. a. (2021). The 2021 report of the lancet countdown on health and climate change: code red for a healthy future. *The Lancet*, *398*(10311), 1619–1662.

Schepanski, K. (2018). Transport of mineral dust and its impact on climate. *Geosciences*, *8*(5), 151.

Schifano, P., Lallo, A., Asta, F., De Sario, M., Davoli, M., & Michelozzi, P. (2013). Effect of ambient temperature and air pollutants on the risk of preterm birth, rome 2001–2010. *Environment international*, *61*, 77–87.

Shah, & et al. (2015). Short term exposure to air pollution and stroke: systematic review and meta-analysis. *bmj*, *350*.

Shahsavani, A., Naddafi, K., Haghighifard, N. J., Mesdaghinia, A., Yunesian, M., Nabizadeh, R., ... et al. (2012). The evaluation of pm10, pm2. 5, and pm1 concentrations during the middle eastern dust (med) events in ahvaz, iran, from april through september 2010. *Journal of arid environments*, *77*, 72–83.

Shao, Y., Wyrwoll, K.-H., Chappell, A., Huang, J., Lin, Z., McTainsh, G. H., ... Yoon, S. (2011). Dust cycle: An emerging core theme in earth system science. *Aeolian Research*, *2*(4), 181–204.

Sivakumar, M. V. (2005). Impacts of sand storms/dust storms on agriculture. In *Natural disasters and extreme events in agriculture: impacts and mitigation* (pp. 159–177).

Springer.

Sorek-Hamer, M., Cohen, A., Levy, R. C., Ziv, B., & Broday, D. (2013). Classification of dust days by satellite remotely sensed aerosol products. *International journal of remote sensing*, *34*(8), 2672–2688.

Stafoggia, M., Zauli-Sajani, S., Pey, J., Samoli, E., Alessandrini, E., Basagaña, X., … et al. (2016). Desert dust outbreaks in southern europe: contribution to daily pm10 concentrations and short-term associations with mortality and hospital admissions. *Environmental health perspectives*, *124*(4), 413–419.

Stefanski, R., & Sivakumar, M. V. (2009). Impacts of sand and dust storms on agriculture and potential agricultural applications of a sdsws. In *Iop conference series: earth and environmental science* (Vol. 7, p. 012016).

Stein, A., Draxler, R. R., Rolph, G. D., Stunder, B. J., Cohen, M., & Ngan, F. (2015). Noaa's hysplit atmospheric transport and dispersion modeling system. *Bulletin of the American Meteorological Society*, *96*(12), 2059–2077.

Sugimoto, N., Uno, I., Nishikawa, M., Shimizu, A., Matsui, I., Dong, X., … Quan, H. (2003). Record heavy asian dust in beijing in 2002: Observations and model analysis of recent events. *Geophysical Research Letters*, *30*(12).

Tan, Z., & Yan, L. (2021). Does air pollution impede corporate innovation? *International Review of Economics & Finance*, *76*, 937–951.

Tang, Q., & Yuan, Z. (2019). Cat bond pricing under a product probability measure with pot risk characterization. *ASTIN Bulletin: The Journal of the IAA*, *49*(2), 457–490.

Team, R. C. (2018). R: A language and environment for statistical computing. 2014. *R Foundation for Statistical Computing: Vienna, Austria.*

Teh, T.-L., & Woolnough, C. (2019). A better trigger: Indices for insurance. *Journal of Risk and Insurance*, *86*(4), 861–885.

Touloumi, G., Samoli, E., Pipikou, M., Le Tertre, A., Atkinson, R., & Katsouyanni, K. (2006). Seasonal confounding in air pollution and health time-series studies: Effect on air pollution effect estimates. *Statistics in medicine*, *25*(24), 4164–4178.

Trasande, L., Malecha, P., & Attina, T. M. (2016). Particulate matter exposure and preterm birth: estimates of us attributable burden and economic costs. *Environmental health perspectives*, *124*(12), 1913–1918.

UNEP, & WMO. (2016). *Global assessment of sand and dust storms* (Tech. Rep.). Nairobi: United Nations Environment Programme.

United Nations ESCAP. (2018). *Sand and dust storms in asia and the pacific: Opportunities for regional cooperation and action* (Tech. Rep.). Bangkok: United Nations Economic and Social Commission for Asia and the Pacific (ESCAP).

Uno, I., Amano, H., Emori, S., Kinoshita, K., Matsui, I., & Sugimoto, N. (2001). Trans-pacific yellow sand transport observed in april 1998: A numerical simulation. *Journal of Geophysical Research: Atmospheres*, *106*(D16), 18331–18344.

Ventusky. (2024, August). *Air quality.* https://www.ventusky.com/?p=38;52;1&l=pm10. (Accessed: August 2023)

Viscusi, W. K., & Masterman, C. J. (2017). Income elasticities and global values of a statistical life. *Journal of Benefit-Cost Analysis*, *8*(2), 226–250.

Von Schneidemesser, E., Monks, P. S., Allan, J. D., Bruhwiler, L., Forster, P., Fowler, D., … et al. (2015). Chemistry and the linkages between air quality and climate change. *Chemical reviews*, *115*(10), 3856–3897.

Wang, J. X. (2015). Mapping the global dust storm records: Review of dust data sources in supporting modeling/climate study. *Current Pollution Reports*, *1*, 82–94.

Wang, Y., Stein, A. F., Draxler, R. R., Jesús, D., & Zhang, X. (2011). Global sand and dust storms in 2008: Observation and hysplit model verification. *Atmospheric environment*, *45*(35), 6368–6381.

Wang, Y., Zhang, X., Gong, S., Zhou, C., Hu, X., Liu, H., … Yang, Y. (2008). Surface observation of sand and dust storm in east asia and its application in cuace/dust. *Atmospheric Chemistry and Physics*, *8*(3), 545–553.

Washington, R., Todd, M., Middleton, N. J., & Goudie, A. S. (2003). Dust-storm source areas determined by the total ozone monitoring spectrometer and surface observations.

Annals of the Association of American Geographers, *93*(2), 297–313.

WHO. (2022, September). *Who global air quality guidelines.* https://www.who.int/publications/i/item/9789240034228.

Williams, P., & Young, M. (1999). *Costing dust: How much does wind erosion cost the people of south australia. final report* (Tech. Rep.). Adelaide: CSIRO Land and Water.

World Bank Treasury. (2019, April). *Super-sized catastrophe bond for earthquake risk in latin america* (Case Study). Washington, DC: World Bank. Retrieved 2025-08-22, from https://thedocs.worldbank.org/en/doc/192341554318525877-0340022019/original/casestudyfinancialproductsPacificAlliancefinal4-1-2019.pdf

World Health Organization. (2019). *International Classification of Diseases, 10th Revision (ICD-10).* Retrieved from https://icd.who.int/browse10/2019/en (Accessed: 2024-08-13)

World Health Organization. (2021). *Review of evidence on health aspects of air pollution: Revihaap project: Technical report* (Tech. Rep.). Copenhagen: World Health Organization, Regional Office for Europe.

World Health Organization. (2024). *Sand and dust storms.* Retrieved from https://www.who.int/news-room/fact-sheets/detail/sand-and-dust-storms (Accessed: 11-Feb-2025)

Yuan, J., Li, M., Lv, G., & Lu, Z. K. (2020). Monitoring transmissibility and mortality of covid-19 in europe. *International Journal of Infectious Diseases*, *95*, 311–315.

Zhang, Y., Wang, J., & Wang, X. (2014). Review on probabilistic forecasting of wind power generation. *Renewable and Sustainable Energy Reviews*, *32*, 255–270.

Zhou, C., Gong, S., Zhang, X., Wang, Y., Niu, T., Liu, H., ... Hou, Q. (2008). Development and evaluation of an operational sds forecasting system for east asia: Cuace/dust. *Atmospheric Chemistry and Physics*, *8*(4), 787–798.

A. DDS Identification Methodology

A.1 Background of DDS identification

Desert Dust storms are documented through a variety of methodologies involving PM_{10} levels, AOD data, actual visibility at the horizon (N. J. Middleton, Goudie, & Wells, 2020; Natsagdorj, Jugder, & Chung, 2003; Y. Wang et al., 2008; Al-Hemoud et al., 2021), the lidar measure extinction coefficient capturing the dust height distribution (Sugimoto et al., 2003), particle matter concentrations observed at ground levels, and different satellite sensor measurements (Washington, Todd, Middleton, & Goudie, 2003; Prospero, Ginoux, Torres, Nicholson, & Gill, 2002; Hu, Lu, Niu, & Zhang, 2008). For example, the Northern Hemisphere ranging from the West coast of North Africa over the Middle East to China has been identified as the major dust source area by the observations of (TOMS) sensor (Prospero, Ginoux, Torres, Nicholson, & Gill, 2002). Additionally, the examination of both global and regional dust storm properties have motivated the development of various dust storm models (Ginoux et al., 2001; Pérez et al., 2006; Uno et al., 2001; Zhou et al., 2008). For the conduction of the current study, the Hybrid Single-Particle Lagrangian Integrated Trajectory (HYSPLIT) model (Draxler & Hess, 1998), is employed, originally applied for the simulation of DDSs and the estimation of PM_{10} concentrations in the areas of Iraq, Saudi Arabia and Kuwait (Draxler, Gillette, Kirkpatrick, & Heller, 2001). Accordingly, a more comprehensive and generalized emission application was version was letter in integrated into HYSPLIT, eliminating any additional requirements regarding digital soil characteristics and was first used for the examination of Northern Africa (Escudero et al., 2006). Subsequently, additional improvements are implemented in HYSPLIT via the integration of a novel empirically derived approach based on observations from MODIS (Moderate Resolution Spectroradiometer) Aerosol Optical Depth (AOD) values, whose ability (Draxler, Ginoux, & Stein, 2010). The ability of the underlined model was originally examined in a global application regime by (Y. Wang, Stein, Draxler, Jesús, & Zhang, 2011) giving emphasis on two primary dust sources namely North Africa and Northeast Asia, for the entire year period of 2008, deriving both seasonal dust variations and global dust spatial distributions.

A.2 Methodology of current paper

A.2.1 Data

A.2.1.1 Ground Observations

Continuous measurements of PM_{10} and $PM_{2.5}$ concentrations are gathered for the examination period from each monitoring station in the ground-monitoring-coverage examined along with hourly records of four meteorological parameters namely temperature, wind speed, precipitation and relative humidity. The data are then aggregated to a daily frequency by taking the daily average value of all days with at least 12 h observations and omitting the remaining days from the data sample. A gravimetric measure is then employed for the replacement of daily missing PM_{10} concentration measures if applicable or by regressing $PM_{2.5}$ concentration data from neighbouring stations using a regression model of the form:

$$PM_{10,i} = \beta_0 + PM_{2.5-Neighbouring,i} + WS_i + Temp_i \quad ,$$

where $PM_{10,i}$ denotes the average 24 h PM_{10} concentration subject to day i, β_0 signifies the regression intercept, $PM_{2.5-Neighbouring,i}$ signifies the daily mean of $PM_{2.5}$ measures from the station in closest proximity for day i, WS_i and $Temp_i$ denote the daily average wind speed and temperature respectively as recorder by station examined for day i.

A.2.1.2 Satellite AOD Observations

Three hourly AOD observations are gathered with wavelength 550nm (Dust-AOD_{550}) through the Copernicus Atmosphere Monitoring Service (CAMS) global reanalysis data set provided by the European Centre for Medium-Range Weather Forecasts (ECMWF) (Inness et al., 2019), covering a wide range of sites with spatial resolution of approximately 80km ($0.7° \times 0.7°$ mesh). The daily (Dust-AOD_{550}) are estimated by aggregating the obtained observations.

A.2.2 Data Analyses

A.2.2.1 DDS Classification

The DDS classification methodology adopted by the current methodology is in line with the methodology outlined by (Sorek-Hamer, Cohen, Levy, Ziv, & Broday, 2013). Specifically, for the construction of the classification model for the identification of DDSs both the upper and lower atmospheric levels are required to be examined via the employment of both satellite AOD products combined with ground level observations respectively. The underlined methodology is outlined by the steps that follow:

(a) Initially, a complete two-year data set analysis is conducted for all sites in the examination area combining Dust-AOD values, PM_{10} concentration values and corrected reflectance images obtained by MODIS - Terra and Aqua satellites - publicly available by the NASA Worldview Application facilitated by the NASA/Goddard Space Flight Centre Earth Science Data and Information System (ESDIS) project `https://worldview.earthdata.nasa.gov/`. Moreover, the daily ratio of $\frac{PM_{10}}{PM_{2.5}}$ along with the elemental concentrations available for each examined station are obtained and furtherly examined for the two years of reference investigated. The rationale behind the outlined methodology lies in the detection of less intensive DDS events, that might have been failed to be officially recorder otherwise and the enhancement of the analysis sensitivity. Specifically, all days within the two years of reference sample are screened subject to the concentration levels of PM_{10}, Dust-AOD values and satellite derived images, depicting excess particle suspension over the ares of investigation, and when applicable the crustal elemental concentration along with the $\frac{PM_{10}}{PM_{2.5}}$ ratio. In the cases where all the aforementioned observations exhibit a peak in the recorder values, the associated calendar days within the reference years are classified as DDS (DDS, dust = 1) denoting the occurrence of a DDS event and non-DDS (NDDS, dust = 0) otherwise.

(b) The next step examines all classified days in the reference years via the application of a Classification and Regression Tree (CART) algorithm. The data employed (dataset A) include the daily concentration levels of PM_{10}, Dust-AOD values, all gathered meteorological variables along with the seasonal categorical variables for the identification of the most optimal set of rules for the classification of DDS and NDDS. The set of explanatory factors imposed as rules for the classification of DDS is determined via the classification tree exhibiting the smallest cross-validation error. Furthermore, the derived set of rules is then used for the transformation of dataset A into a binary detest B by applying the algorithm for each geolocation examined independently.

(c) Building upon the reference years methodology, DDS and N*DDS days* are identified in the remaining examination years through the application of a Logistic Regression Model for the approximation of the relevant threshold and daily probability values. In particular, the days with the probability of a DDS occurrence greater than the threshold value are classified as DDS (dust = 1) and vice-versa. The probability of DDS is given by the following logistic regression model:

$$Logit(P) = ln\left(\frac{P}{1-P}\right) = \beta_0 + \beta_1 x_1 + \beta_2 x_2 + ... + \beta_i x_i \quad ,$$

where P denotes the probability of occurrence of a DDS, β_0 signifies the regression intercept and β_i denotes the regression coefficient associated with each rule x_i derived through the CART model. For the evaluation of the logistic regression model performance, dataset B is divided into two subsets the former of which includes 80% of the observations denoting the training subset, and the latter of which includes the remaining 20% of the observations signifying the testing subset on which the model evaluation is performed. The underlined process is then repeated 10 times, each time with a different randomly selected training and testing subsets, from which the relation of true positive rate (sensitivity; true when DDS is identifies as DDS) against the false positive rate (1-specificity: true NDDS where incorrect identified as DDS) is graphically illustrated deriving the so called Receiver Operator Characteristic (ROC) curve. The optimal threshold value is then obtained from the ROC curve based on two criteria. The former includes the former includes the Youden index maximizing the sum of sensitivity and specificity denoting the true negative rate denoting the correct true NDDS classification and the latter of which includes the curve point with closest proximity to the (0,1) axis value. The regression coefficients used from the 10 runs are the ones that yield the greatest accuracy when verified with the testing dataset and similarly the optimal threshold values are specified according to the average ROC curve independently for each station in the sample.

(d) Finally, the combined CRAT regression is implemented on all the days included in the entire examination period deriving the finalized DDS and NDDS classification of the sample. Days with missing PM_{10} concentration data are treated in a similar manner to the years of reference.

(e) As a robustness check and for the determination of the aerolian dust source of origin, the 5-day backward air trajectories are examined using the Hybrid Single Particle Lagrangian Integrated Trajectory (HYSPLIT) model for the altitudes of 500, 15,000 and 25,000 height above ground level (Stein et al., 2015; Rolph, Stein, & Stunder, 2017).

A.2.2.2 Non-parametric Trend Analysis

The linear trends of DDS events are examined using the Theil-Sen estimator and Mann-Kendall test of significance. Additionally, the non-linear trends of both PM_{10} concentrations and Dust-AOD are furtherly examined using a Generalised Additive Model (GAM) obtaining a time-dependent penalised regression spline function denoted by:

$$\mu_i = \beta_0 + f_i(DDS_i) \quad ,$$

where μ_i signifies either the daily mean PM_{10} concentrations or the Dust-AOD value subject to the DDS day i. Similarly, β_0 represents the regression intercept and $f()$ denotes the penalized regression spline function with degrees of freedom proportional to the smoothing parameter of the Generalized Cross Validation criterion (GCV). The analysis is conducted using the R statistical software supporting the relevant “splines ”, “trend”, “Kendall” and “mgvc” packages (Team, 2018).

B. Economic Costs of DDS events

The economic implications and costs suffered by DDS events can be categorized as either short-term (e.g. premature deaths, hospital admissions and business interruption) or long-term. Both long- and short-term health implications to elevated PM exposures impact the burden of disease, through the amplification of the years of life lost, mortality risk and years lived with disability of the exposed population (Ostro & et al., 2004). Specifically, (Trasande, Malecha, & Attina, 2016) estimate the economic costs attributable to $PM_{2.5}$ exposure in the US in year 2010 via the observation of direct medical costs and lost economic productivity, due to the increased burdens of preterm birth associated with prolonged PM concentration exposure. The incurred findings suggest that the $PM_{2.5}$ attributable costs for 2010 in the US alone reached \$5.09 billion. Similarly (Dechezleprêtre, Rivers, & Stadler, 2019), suggest that air-pollution results to economy-wide reductions in market activity, concluding that a marginal increase of 1 μgm^{-3} in $PM_{2.5}$ concentration correlates with an approximate reduction of 0.8% in real Gross Domestic Product (GDP) in the same year. Focusing on DDS events, only a few studies have attempted to quantify the associated economic costs, which we list in Table B1.

Table B1: Economic costs estimates associated with DDS events.

Estimation	Geographical Area	Cost (US\$)	Reference
Total Costs	Beijing, China	265m	(Ai & et al., 2008)
Total Costs	Iran	1,0bn	(Meibodi & et al., 2015)
Total Costs	Iraq	1,4bn	(Meibodi & et al., 2015)
Off-site Costs	Seistan Region, Iran	25m	(Miri & et al., 2009)
Off-site Costs	South Australia	17m	(Williams & Young, 1999)
Total Costs	South Korea	5,6bn	(Jeong & et al., 2008)
Off-site Costs	USA	9,6bn	(Pimentel & et al., 1995)
Total Costs	Yartz Plain, Iran	6,8m	(Ekhtesasi & Sepehr, 2009)

The quantification of the net economic costs attributed to PM pollution is not a trivial task as it involves the quantification of all transmission channels through which excess PM concentrations impact economic sectors such as human health, business activity, productivity and the environment. Specifically, DDS can interrupt business activity, reduce labor productivity, impact innovation, halt transportation, damage infrastructure and crop yields (Cavalcanti, Mohaddes, Nian, & Yin, 2023; Tan & Yan, 2021; N. J. Middleton, 2017).[17]

Moreover, it might impact sectors such as agriculture, as it might impact livestock health (Stefanski & Sivakumar, 2009; N. Middleton, 2024), and also photosynthesis production for plants (Sivakumar, 2005; Schepanski, 2018).

A significant body of literature focuses on the impact of the PM components of air pollution on human health. There is ample evidence of the adverse effects of PM_{10} exposure (Mukherjee & Agrawal, 2017) on human health (World Health Organization, 2021) including the amplification of ischemic heart disease (Zhang, Wang, & Wang, 2014), DNA degradation (Coronas et al., 2009) and increased preterm birth risk (Schifano et al., 2013). Additionally, the WHO Air quality guidelines report (WHO, 2022) along with several recently conducted systematic reviews, meta-analyses and time-series studies identify the effect of PM pollution on both all-cause, cause-specific mortality and hospital admissions (Bell, Zanobetti, & Dominici, 2013; Atkinson & et al., 2014; R. W. Atkinson, Mills, Walton, & Anderson, 2015; Shah & et al., 2015; Liu et al., 2019).

[17]Examples of severe DDS events are one in Phoenix (Arizona, USA) in 2011 (National Geographic, 2011), and another one in Cyprus (2015) (CNN, 2011; NASA Earth Observatory, 2015), that resulted in flight cancellations and disrupting business activity.

C. PM_{10} and Health Outcomes Seasonality Trends

Table C1 describes the distribution of DDS and non-*DDS days* across different days of the week alongside the associated average PM_{10} concentration levels and corresponding p-values. Once again, data depict homogeneous patterns throughout the week, with elevated PM_{10} concentrations on *DDS days* as oppose to non-*DDS days* for every weekday (Monday to Friday), as well as weekends (Saturday and Sunday). For example, Mondays display an average PM_{10} concentration of 59.758 μg/m^3 on *DDS days*, whilst the average average PM_{10} concentration on non-*DDS days* is significantly lower taking the value of 18.086 μg/m^3, as suggested by reported the p-value. This trend propagates across all days of the week, signifying the consistent association between DDS and inflated PM_{10} levels irrespective of the weekday.

Table C1: Summary table of total *DDS days* per day of the week in sample, total hospitalizations for DDS=1, DDS=0, and all days for each day of the week.

Day of Week	Total Days DDS=1	Average PM_{10} con.			P-value
		for DDS=1 (μg/m^3)	for DDS=0 (μg/m^3)	Total Average PM_{10} con.	
Monday	104	59.758	18.086	25.729	<0.001
Tuesday	96	61.764	17.921	25.357	<0.001
Wednesday	88	51.752	18.438	23.590	<0.001
Thursday	93	49.687	18.568	23.635	<0.001
Friday	105	60.765	18.256	26.067	<0.001
Saturday	112	58.705	18.361	26.301	<0.001
Sunday	112	57.760	18.182	26.042	<0.001

Finally, Table C2 delineates the outputs of ANOVA and Kruskal-Wallis tests investigating the association between total deaths and hospital admissions with the seasonality trends of day of the week and season. Regarding total hospitalizations, both ANOVA and Kruskal-Wallis tests yield extremely low p-values, suggesting a significant association between hospitalizations and day of the week as well as hospitalizations and season. Similarly, in regards to total deaths, whilst the ANOVA tests indicate a lessen significant association, the Kruskal-Wallis tests indicate a robust association between deaths and both seasonality factors. The underlined findings underscore the significance of considering temporal factors (day of the week and season) in the time series analysis examining health outcomes related to air quality and specifically DDS.

Table C2: Summary of ANOVA and Kruskal-Wallis test results for total deaths and total hospitalizations by day of the week and season.

Variable	Test Type	Test Statistic	p-value
Total Deaths by Day of the Week			
Day of the Week	ANOVA	1.993	0.0632
	Kruskal-Wallis	10.948	0.08998
Total Hospitalizations by Day of the Week			
Day of the Week	ANOVA	263.3	$< 2 \times 10^{-16}$
	Kruskal-Wallis	1221.5	$< 2.2 \times 10^{-16}$
Total Deaths by Season			
Season	ANOVA	174.6	$< 2 \times 10^{-16}$
	Kruskal-Wallis	417.96	$< 2.2 \times 10^{-16}$
Total Hospitalizations by Season			
Season	ANOVA	145.7	$< 2 \times 10^{-16}$
	Kruskal-Wallis	339.18	$< 2.2 \times 10^{-16}$

D. Cyprus: The Impact of *DDS days* on daily number of hospital admissions

We requested hospitalization data subject to cardiovascular and respiratory-specific diseases from the Ministry of Health of Cyprus for the time period starting on January 2007 up to 2017, attaining a total number of observation of 3820. The mean and median values of the aggregated sum of both respiratory and cardiovascular daily hospital admissions, captured by *Total Hosp.* are 33.42 and 32 respectively, with interquantile range between 23 and 42 hospitalizations per day and a standard deviation of approximately 13.6 daily hospitalizations. Comparable figures are also reported for both the *Respiratory* and *Cardiovascular* variables with the latter experiencing more variability.

We show the results of the impact of DDS on daily hospitalizations in Table D1. Panel A includes *DDS days* as classified by (Achilleos et al., 2020), whilst Panel B reports the results of the differentiated *DDS days*, namely DDS_{mild} and DDS_{severe}. The first column outlines the impact of DDS on total hospitalizations expressed as the aggregated sum of respiratory specific hospitalizations, reported in the second column, and cardiovascular specific hospitalizations reported in the third column. The estimated coefficients in Panel A show a positive and statistically significant (p-value < 0.01) impact of *DDS days* on the daily total number of hospitalizations. The size of the coefficient is also economically significant as the logarithm of the total daily hospitalizations is expected to increase by 6.6% during *DDS days*, which translates to an expected increase of 6.8% in total hospitalizations. The obtained effect appears to be driven by both respiratory and cardiovascular specific hospitalizations as both estimates are statistically and economically significant (p-values < 0.01). The impacts of *DDS* on daily hospitalizations subject to respiratory and cardiovascular causes equal to an increase of magnitude 9.1% and 5% respectively.

Similarly, the estimated coefficients in Panel B of DDS_{mild} and DDS_{severe} show a positive and statistical significant impact on the daily number of total hospitalizations (p-values < 0.01). The expected increase of total daily hospitalization on *Mild DDS days* equals 6.8% whilst the increase in total daily deaths on *Severe DDS days* equals 8.1%.

The effect of DDS_{mild} appears to be driven by daily deaths associated with both respiratory and cardiovascular causes with the coefficients DDS_{mild} being statistically significant suggesting an expected increase of 8.8% in respiratory and 5.2% in cardiovascular specific hospitalizations. The impact of DDS_{severe} materializes primarily from respiratory related hospitalizations as the DDS_{severe} is statistically insignificant for cardiovascular causes. The obtained findings are in agreement with the results reported in Table 5 Panel B, verifying the proposed explanation that Severe DDS induce more cardiovascular specific fatalities as the impact of DDS_{severe} on cardiovascular related hospitalizations is statistically not different from zero.

Table D1: Impact of DDS on daily hospital admissions.

This table uses a Generalized Additive Model (GAM) regression for the examination of the impact of DDS on the daily count hospital admissions. The dependent variables include (a) the logarithm of the aggregated total of daily hospitalizations subject to respiratory and cardiovascular diseases *Total Daily Hospitalizations*, (b) the logarithm of daily number of hospital admissions subject to respiratory diseases *Respiratory*, (c) the logarithm of daily number of hospital admissions subject to cardiovascular diseases *Cardiovascular*. The dataset ranges from January 2007 up to December 2017. Panel A reports the results of the binary parametric coefficient DDS that equals one on *DDS days* and zero otherwise. Panel B reports the results of the binary parametric coefficients DDS_{mild} and DDS_{severe}. The former variable is defined as all the *DDS days* from the original dataset with PM_{10} daily concentrations less than 165 $\mu g/m^3$, whilst the latter is defined as the remaining *DDS days* with daily PM_{10} concentrations above the specified threshold. The non-linear effects of the lagged relative humidity and lagged temperature on the dependent variable are captured through the spline functions $s(RelHum_{lag1})$ and $s(Temp_{lag1})$ respectively. The model accounts for fixed effects related to the - day of the week, season and year. The coefficient estimate of each explanatory variable is reported along with the associated $p-$value in both Panel A and Panel B. *, **, and *** signify the statistical significance at the 10%, 5% and 1% level respectively. The analysis has been carried out using different threshold specifications and the incurred findings remain qualitatively the same.

Panel A

	Total Daily Hospitalizations		Respiratory		Cardiovascular	
	Estimate	p-value	Estimate	p-value	Estimate	p-value
Parametric Coefficients						
Intercept	-57.57	$< .01$ ***	-51.84	$< .01$ ***	-63.81	$< .01$ ***
DDS	0.066	$< .01$ ***	0.087	$< .01$ ***	0.049	$< .01$ ***
Smooth Terms						
s(RelHum_lag1)	6.714	$< .01$ ***	7.776	$< .01$ ***	3.188	$< .01$ ***
s(Temp_lag1)	8.290	$< .01$ ***	7.881	$< .01$ ***	7.863	$< .01$ ***
Model Fit Statistics						
Adjusted R^2	0.462		0.463		0.344	
Deviance Explained	47%		48.7%		33.8%	
n	3820		3820		3820	

Panel B

	Total Daily Hospitalizations		Respiratory		Cardiovascular	
	Estimate	p-value	Estimate	p-value	Estimate	p-value
Parametric Coefficients						
Intercept	-57.56	$< .01$ ***	-51.79	$< .01$ ***	-63.84	$< .01$ ***
DDS_{mild}	0.066	$< .01$ ***	0.085	$< .01$ ***	0.051	$< .01$ ***
DDS_{severe}	0.078	0.030 **	0.155	$< .01$ ***	-0.000	0.994
Smooth Terms						
s(RelHum_lag1)	6.701	$< .01$ ***	7.734	$< .01$ ***	3.190	$< .01$ ***
s(Temp_lag1)	8.290	$< .01$ ***	7.888	$< .01$ ***	7.859	$< .01$ ***
Model Fit Statistics						
Adjusted R^2	0.462		0.463		0.344	
Deviance Explained	47%		48.7%		33.8%	
n	3820		3820		3820	

Table D2: Impact of DDS on daily hospitalizations including lagged effects. This table uses a Generalized Additive Model (GAM) regression for the examination of the impact of DDS on the daily count of hospitalizations. The dependent variables include, (a) the logarithm of the aggregated total of daily hospitalizations subject to respiratory and cardiovascular diseases *Total Daily Deaths*, (b) the logarithm of daily number of hospitalizations subject to respiratory diseases *Respiratory*, (c) the logarithm of daily number of hospitalizations subject to cardiovascular diseases *Cardiovascular*. The dataset ranges from January 2007 up to December 2017. Panel A reports the results of the binary parametric coefficient DDS that equals one on **DDS days** and zero otherwise along with the results of the $DDS_{crossbasis}$ indicator that captures the 7-day lagged effects of DDS on the dependent variable. Panel B reports the results of the binary parametric coefficients DDS_{mild} and DDS_{severe}. The former variable is defined as all *DDS days* from the original dataset with PM_{10} daily concentrations less than 165 $\mu g/m^3$, whilst the latter is defined as the remaining *DDS days* with daily PM_{10} concentrations above the specified threshold. The 7-day lagged effects subject to DDS are captured by the binary variables $DDS_{crossbasis\ mild}$ and $DDS_{crossbasis\ severe}$ respectively. The non-linear effects of the lagged relative humidity and lagged temperature on the dependent variable are captured through the spline functions $s(RelHum_{lag1})$ and $s(Temp_{lag1})$ respectively. The model accounts for fixed effects related to the day of the week, season and year. The coefficient estimate of each explanatory variable is reported along with the associated $p-$value in both Panel A and Panel B. *, **, and *** signify the statistical significance at the 10%, 5% and 1% level respectively. The analysis has been carried out using different threshold specifications and the incurred findings remain qualitatively the same.

Panel A

	Total Daily Hospitalizations		Respiratory		Cardiovascular	
	Estimate	p-value	Estimate	p-value	Estimate	p-value
Parametric Coefficients						
Intercept	-59.53	< .001 ***	-53.68	< .001 ***	-65.96	< .001 ***
DDS	0.040	< .001 ***	0.058	< .001 ***	0.025	0.031 **
$DDS_{cross-basis}$	0.009	< .001 ***	0.006	0.062 *	0.012	0.001 **
Smooth Terms						
s(RelHum_lag1)	6.527	< .001 ***	7.427	< .001 ***	3.104	< .001 ***
s(Temp_lag1)	8.283	< .001 ***	7.837	< .001 ***	-	-
Model Fit Statistics						
Adjusted R^2	0.499		0.521		0.353	
Deviance Explained	50.1%		53.2%		34.7%	
n	3856		3856		3856	

Panel B

	Total Daily Hospitalizations		Respiratory		Cardiovascular	
	Estimate	p-value	Estimate	p-value	Estimate	p-value
Parametric Coefficients						
Intercept	-59.12	< .001 ***	-52.54	< .001 ***	-66.31	< .001 ***
DDS_{mild}	0.050	< .001 ***	0.075	< .001 ***	0.029	0.016 **
DDS_{severe}	0.039	0.304	0.148	0.005 ***	-0.069	0.204
$DDS_{crossbasis\ mild}$	0.008	< .001 ***	0.008	0.045 **	0.010	0.005 **
$DDS_{crossbasis\ severe}$	0.024	0.122	-0.008	0.720	0.05	0.014 **
Smooth Terms						
s(RelHum_lag1)	224.3	< .001***	162.8	< .001 ***	84.38	< .001 ***
s(Temp_lag1)	294.6	< .001 ***	280.6	< .001 ***	132.5	< .001 ***
Model Fit Statistics						
Adjusted R^2	0.471		0.469		0.35	
Deviance Explained	48.0%		49.3%		34.5%	
n	3628		3628		3628	

Table D2 Panel A illustrates the results of the impact of DDS on the daily number of total hospitalizations, following the model specification of Equation 4.2. The results are qualitatively the same as in Table 7. Unlike the results outlined in Table 5, the introduction of $DDS_{cross-basis}$ appears to have a deflating effect on the DDS coefficients, which remain however statistically significant (p-values <0.1) for total, respiratory and cardiovascular (p-value <0.05) specific hospitalizations. Specifically, *DDS days* are expected to increase total daily hospitalizations by 4.1%, and by 6% and 2.6% respiratory and cardiovascular specific daily hospitalizations compared to *non DDS days.* The coefficients of $DDS_{cross-basis}$ are statistically significant (p-value $<$ 0.01), (p-value <0.1), (p-value <0.05) for total, respiratory and cardiovascular specific hospitalizations respectively. The obtained results suggest a complementary effect on hospitalization outcomes that is driven not by *DDS days* but rather by the subsequent 7 days from the DDS day. These lagged effects captured by $DDS_{crossbasis}$ have significant economic implications as healthcare systems can leverage this information to better prepare and manage capacity planing and resource allocation over the days following DDS events.

These findings align with Panel B reporting the impact of DDS_{mild}, DDS_{severe} along with the impact of the corresponding lagged effect coefficients $DDS_{crossbasis-mild}$ and $DDS_{crossbasis-severe}$ on hospitalization outcomes. The coefficient of DDS_{mild} is statistically significant for all hospitalization outcomes (p-values $<$ 0.01) for total and respiratory specific hospitalizations and for cardiovascular related hospital admissions (p-value $<$ 0.05). The net effect of DDS_{mild} on total hospitalization is captured by an increase of 5.1% which is attributed to the increase of 7.8% for respiratory and 2.5% for cardiovascular related hospitalizations. Similarly, the coefficient of DDS_{severe} is statistically significant only for respiratory related hospital admissions (p-value $<$ 0.01) and equals to 0.148 denoting an expected increase in hospitalizations of $\approx$ 16% when $DDS_{severe} = 1$. Finally, the lagged effect coefficients of $DDS_{crossbasis\,mild}$ are statistically significant across all hospitalization outcomes with (p-values <0.05) whilst the coefficient of DDS_{severe} is only statistically significant (p-value $<$ 0.05) for cardiovascular specific hospitalizations, denoting the increased sensitivity of cardiovascular hospital admissions to greater daily PM_{10} concentration levels.

E. Italy Lag-Structure GAM Model Results

Table E1: Impact of Variables on Total Deaths per NUTS-2 Code

Generalized Additive Model (GAM) regressions examining the impact of DDS on daily deaths. The dependent variable is given by the logarithm of the aggregated daily counts of death subject to respiratory and cardiovascular causes. The non-linear effects of the lagged temperature and lagged relative humidity on total deaths are captured via the spline functions s(lag1_temp) and s(lag1_RH) respectively. The model incorporates fixed effects related to the day of the week, season, and year. The estimated coefficient of each independent variable is reported along with the associated p-value. *, **, and *** signify statistical significance at the 10%, 5%, and 1% levels respectively.

	ITC1		ITG2		ITH5		ITI4	
	Estimate	p-value	Estimate	p-value	Estimate	p-value	Estimate	p-value
Parametric Coefficients								
(Intercept)	-7.777	< 0.001 ***	-5.607	0.0117 **	2.082	0.149	-19.21	< 0.001 ***
DDS	-0.004	0.609	-0.017	0.184	-0.018	0.018 **	0.005	0.445
$DDS_{cross-basis}$	0.022	< 0.001 ***	0.024	< 0.001 ***	0.020	< 0.001 ***	0.018	< 0.001 ***
Smooth Terms								
s(temp_lag1)	7.589	< 0.001 ***	7.889	< 0.001 ***	6.411	< 0.001 ***	8.387	< 0.001 ***
s(RH_lag1)	7.348	< 0.001 ***	3.466	0.201	4.692	< 0.001 ***	5.447	0.00126 **
Model Fit Statistics								
Adjusted R^2	0.413		0.269		0.394		0.465	
Deviance Explained	42.4%		27.2%		40.1%		47.5%	
n	4212		3878		3814		3909	

E.1 Italy Lag-Structure GAM Model Results for DDS_{Severe} and DDS_{Mild}.

Table E2: Impact of Variables on Total Deaths per NUTS-2 Code

Generalized Additive Model (GAM) regressions examining the impact of DDS on daily deaths. The dependent variable is given by the logarithm of the aggregated daily counts of death subject to respiratory and cardiovascular causes. The non-linear effects of the lagged temperature and lagged relative humidity on total deaths are captured via the spline functions s(lag1_temp) and s(lag1_RH) respectively. The model incorporates fixed effects related to the day of the week, season, and year. The estimated coefficient of each independent variable is reported along with the associated p-value. *, **, and *** signify statistical significance at the 10%, 5%, and 1% levels respectively.

	ITC1		ITG2		ITH5		ITI4	
	Estimate	p-value	Estimate	p-value	Estimate	p-value	Estimate	p-value
Parametric Coefficients								
(Intercept)	-7.584	< 0.001	-5.447	0.014 **	2.081	0.150	-19.140	< 0.001 ***
DDS_{Severe}	0.014	0.659	0.076	0.185	0.036	0.279	0.059	0.067*
DDS_{Mild}	-0.004	0.540	-0.019	0.126	-0.017	0.023 **	0.004	0.542
$DDS_{Severe_{cross-basis}}$	-0.010	0.563	0.057	0.047 **	0.052	< 0.001 ***	0.035	0.015 **
$DDS_{Mild_{cross-basis}}$	0.023	< 0.001 ***	0.023	< 0.001 ***	0.018	< 0.001 ***	0.017	< 0.001 ***
Smooth Terms								
s(temp_lag1)	7.598	< 0.001 ***	7.902	< 0.001 ***	6.453	< 0.001 ***	8.397	< 0.001 ***
s(RH_lag1)	7.336	< 0.001 ***	3.439	0.229	4.796	< 0.001 ***	5.380	0.003 ***
Model Fit Statistics								
Adjusted R^2	0.413		0.271		0.397		0.465	
Deviance Explained	42.400%		27.400%		40.300%		47.600%	
n	4212		3878		3814		3909	